DEPARTMENT OF PHYSICS
UNIVERSITY OF JYVÄSKYLÄ
RESEARCH REPORT No. 5/2017

RARE BETA DECAYS AND THE SPECTRUM-SHAPE METHOD

BY
MIKKO HAARANEN

Academic Dissertation
for the Degree of
Doctor of Philosophy

To be presented, by permission of the
Faculty of Mathematics and Natural Sciences
of the University of Jyväskylä,
for public examination in Auditorium FYS 1 of the
University of Jyväskylä on September 28, 2017
at 12 o'clock noon

Jyväskylä, Finland
September 2017

ISBN 978-951-39-7154-0

Preface

The work presented in this thesis has been carried out at the Department of Physics, University of Jyväskylä during the years 2013-2017. The work was supported by the Academy of Finland under the Finnish Center of Excellence Program 2012-2017 (Nuclear and Accelerator Based Program at JYFL). Financial support from the Finnish Cultural Foundation is also acknowledged.

I want to thank my supervisor, Professor Jouni Suhonen, for his adept and patient guidance during the years of my doctoral studies. I had the great pleasure to start my work with him already as an MSc student. It is fascinating to see how the topic suggested by my supervisor at that time, the theoretical study of rare beta decays, turned out to be such an exciting journey.

Aside from the other collaborators of this thesis, Professor Osvaldo Civitarese and Professor Vladimir Tretyak, who kindly offered to review the original manuscript, I also wish to address my gratitude towards all my friends and colleagues at the field of nuclear and particle research. Thank you for the interesting discussions and memorable moments that we shared together. I will add my thanks to the department staff. It was always a privilege to work around these competent people.

Lastly, I wish to thank my parents and my brother. A special thanks goes to May Ann, my newly married wife. The encouragement and support I received from them far exceeds anything one can hope for.

Jyväskylä, August 2017

Mikko Haaranen

Abstract

This is a thesis consisting of seven publications and an introductory part on theoretical studies on rare single beta decays.

Firstly, the theoretical framework is applied to the computation of partial half-lives for few selected cases of rare single beta-decay transitions. This includes the study on a possible ultra-low-Q-value decay branch of ^{115}Cd as well as the highly forbidden beta decays of ^{48}Ca and ^{50}V. The double magic ^{48}Ca is one of the few experimentally verified nuclei that decay via the two-neutrino mode of double beta decay. A theoretical study on the single beta-decay branches was used to inspect the competition between the single and double beta-decay channels. In the case of ^{50}V the theoretical framework is used to examine the detectability of the beta-minus decay branch that leads to the first excited 2^+ state of ^{50}Cr.

To access the finer details of the theory the usual analysis of beta-decay transitions is extended by the introduction of the next-to-leading-order terms of the beta-decay shape factor. A comparison between the leading-order and the next-to-leading-order contributions is performed in the case of the fourth-forbidden decay branches of ^{113}Cd and ^{115}In.

Finally, an overview on the recently introduced spectrum-shape method is given. The spectrum-shape method (SSM) was developed for the extraction of the effective values of the weak coupling constants as a complementary approach to the usual partial half-life considerations. Highly encouraging results are obtained when SSM is applied to the beta decay of ^{113}Cd. In this initial application of the method consistent values of the two coupling constant were found when the calculations were performed using three different nuclear models.

Author's address Mikko Haaranen
Department of Physics
University of Jyväskylä
Finland

Supervisor Professor Jouni Suhonen
Department of Physics
University of Jyväskylä
Finland

Reviewers Professor Osvaldo Civitarese
Department of Physics
University of La Plata
Argentina

Professor Vladimir Tretyak
Lepton Physics Department
Institute for Nuclear Research
Ukraine

Opponent Professor Fedor Šimkovic
Department of Nuclear Physics and Biophysics
Comenius University
Slovakia

List of Publications

I M. Haaranen, and J. Suhonen, *Beta decay of ^{115}Cd and its possible ultra-low Q-value branch*, Eur. Phys. J. A (2013) **49**: 93

II M. Haaranen, M. Horoi, and J. Suhonen, *Shell-model study of the 4th- and 6th-forbidden β-decay branches of ^{48}Ca*, Phys. Rev. C **89**, 034315 (2014)

III M. Haaranen, P. C. Srivastava, J. Suhonen, and K. Zuber, *β-decay half-life of ^{50}V calculated by the shell model*, Phys. Rev. C **90**, 044314 (2014)

IV M. Alanssari, D. Frekers, T. Eronen, L. Canete, J. Dilling, M. Haaranen, J. Hakala, M. Holl, M. Ješkovský, A. Jokinen, A. Kankainen, J. Koponen, A. J. Mayer, I. D. Moore, D. A. Nesterenko, I. Pohjalainen, P. Povinec, J. Reinikainen, S. Rinta-Antila, P. C. Srivastava, J. Suhonen, R. I. Thompson, A. Voss, and M. E. Wieser, *Single and Double Beta-Decay Q Values among the Triplet ^{96}Zr, ^{96}Nb and ^{96}Mo*, Phys. Rev. Lett. **116**, 072501 (2016)

V M. Haaranen, P. C. Srivastava, and J. Suhonen, *Forbidden nonunique β decays and effective values of the weak coupling constants*, Phys. Rev. C **93**, 034308 (2016)

VI M. Haaranen, J. Kotila, and J. Suhonen, *Spectrum-shape method and the next-to-leading-order terms of the β-decay shape factor*, Phys. Rev. C **95**, 024327 (2017)

VII J. Kostensalo, M. Haaranen, and J. Suhonen, *Electron spectra in forbidden β decays and the quenching of the weak axial-vector coupling constant g_{A}*, Phys. Rev. C **95**, 044313 (2017)

The author has written a computer code for the calculation of the beta-decay partial half-lives using the second-order terms of the beta-decay shape factor. The author has performed the theoretical single beta-decay calculations for the listed publications, except VII. The author has written the first draft of publications I, II, III, V and VI. The author has contributed to conference proceedings where results of the listed publications are presented and discussed.

Contents

1 Introduction

The general features of nuclear single beta decay are usually regarded to be relatively well-established and tested throughout the nuclear landscape. Despite being somewhat overlooked for awhile there has recently been growing interest towards this decay process. Much of the present rediscovery is explained, firstly, by the application of the theory to the more rare types of single beta decays (check e.g. Refs. [1, 2, 3, 4]) that were previously left aside from scientific interest. Secondly, however, the surge of interest is linked to the research on other fields of nuclear physics. Most notable of these are the studies performed on double beta decay (Refs. [5, 6, 7, 8]) and neutrinos (Refs. [5, 9, 10, 11]).

The rare single beta decays are generally characterized by extensively long partial half-lives. This leaves them prone to the hindrance of other decay processes. The retardation of the rare beta decays follows essentially from two unfavourable characteristics: (1) the Q-value of the decay is low, leaving the transition phase space small, and/or (2) there is a large angular-momentum change between the initial and final nuclear states. The extreme cases of type (1) decays are called the *ultra-low-Q-value* transitions. Despite lacking a thoroughly sound definition, the term "ultra-low" typically refers to beta decays with Q-values less than 100 keV (see the discussion e.g. in Ref. [12]).

Decays falling into the category (2) are called the highly *forbidden* transitions. A vast majority of the observable beta decays are either *allowed* or transitions of low forbiddenness. Although these decays are strongly favoured a suitable nuclear structure mismatch between the initial and final nuclear states can sometimes leave only the higher-forbidden channels open. Such decays are found e.g. in nuclei ^{113}Cd and ^{115}In (see Refs. [1, 13]). In both cases the transition is fourth forbidden. However, due to the low decay probabilities in general, the highly-forbidden transition are sometimes challenged even by some higher-order processes. In the case of ^{48}Ca (see Refs. [3, 14]) and ^{96}Zr (e.g. Ref. [15]) the two-neutrino mode of double beta decay is, in fact, found to be the stronger decay channel.

A well-recognized property related to the single beta decay is the mixing of the vector and axial-vector parts in the hadronic current. The effective values of the related coupling constants are not well known in atomic nuclei. Thus any practical calculations are invariably plagued by uncertainties surrounding the values the weak coupling constant. These constant, g_{V} and g_{A}, enter the

theory of nuclear beta decay as means of renormalizing the hadronic current [16, 17, 18]. In addition to the difficulties faced when trying to establish well-defined values to these constants, the unknown value of g_{A}, in particular, casts a shadow also on the studies of double beta decay. While the decay rate of a unique single beta-decay transition is proportional to the second power of g_{A}, this dependence is g_{A}^4 for double beta decays [5, 6]. Such a strong dependence on the axial-vector coupling leaves the experiments aiming to discover the neutrinoless mode of double beta decay highly susceptible to the uncertainties associated with the values of these coupling constants.

The effective values of the weak coupling constants are usually probed by the studies on single beta-decay and two-neutrino double beta-decay partial half-lives (see the discussion in Sect. 3.4). However, the values of the weak coupling constants affect also other beta-decay observables. In particular, a strong effect on the shape of the electron (positron) spectrum, i.e. the beta spectrum, was observed in the study performed in Ref. [1]. The discoveries reported in Ref. [1] led to the introduction of the spectrum-shape method (SSM) that was further studied in Refs. [2, 19]. Based on the encouraging initial results, SSM seems to offer an interesting complement to the usual partial half-life considerations when extracting the effective values of the weak coupling constants.

2 Theory of the nuclear beta decay

In nuclear beta-minus decay the binding energy of a neutron-rich nucleus is increased by a conversion of a single neutron into a proton. The opposite process, i.e. the beta-plus decay, can take place in a proton-rich nucleus. In either case this conversion is associated with an emission of a lepton pair that together carry away the difference ΔJ between the angular momenta of the initial and final nuclear states.[1] The higher the required angular momentum transfer ΔJ, the longer the partial half-life of the corresponding transition becomes.

The angular-momentum transfer and the relative parities of the initial and final nuclear states are used to classify the beta-decay transitions. The decays with $\Delta J = 0, 1$ and no change of parity are called the *allowed* transitions. When the value of ΔJ is higher and/or there is a change of parity between the initial and final nuclear states, the decays are called *forbidden*. The categorization to the 1st-, 2nd-, 3rd-, etc. forbidden decays is done according to the selection rules of Table 2.1.

Forbidden decays with a stretched angular momentum transfer $\Delta J = K+1$ are called *unique* transitions. The ones with unstretched angular momenta, i.e. $\Delta J = K$, are *non-unique*. An increase of the level of forbiddenness by one unit typically corresponds to an increase of partial half-life by several orders of magnitude.

Table 2.1: Selection rules for the forbidden beta decays. K is the level of forbiddenness.

K	1	2	3	4	5	6
ΔJ	0,1,2	2,3	3,4	4,5	5,6	6,7
$\pi_i\pi_f$	-1	+1	-1	+1	-1	+1

[1] The unit $\hbar = h/2\pi$ is usually omitted when referring to angular momentum or angular momentum transfer. Therefore it is customary to write the angular momentum simply as a positive integer or half-integer number L instead of $L\hbar$.

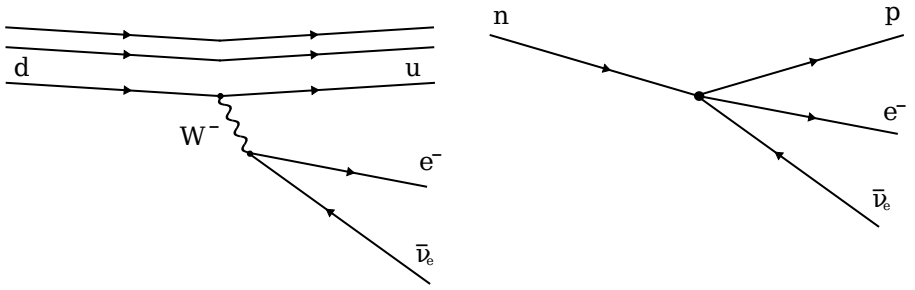

Figure 2.1: Feynman graphs depicting the beta-minus decay. The flavour change of the d quark is presented in the lefthand figure. The righthand figure shows the simplified decay mechanism when the gauge-boson propagation is neglected.

2.1 V-A structure of the weak currents

On the particle level (see Fig. 2.1) beta decay proceeds via the change of quark flavour. This is a weak-interaction process mediated by a gauge boson W. In beta-minus decay one of the u quarks of the decaying nucleon is converted into a d quark, while in the beta-plus decay the opposite takes place. To conserve the electric charge the gauge boson has to have a positive electric charge in the beta-plus decay and negative charge in beta-minus decay. When the gauge boson itself decays it is converted into a lepton pair. Thus the decay process is associated with the emission of either an electron and an electron anti-neutrino, or a positron and an electron neutrino.

The first successful attempt to lay out the beta-decay mechanism was inspired by the structure of the electromagnetic interaction [20]. Both the hadrons and leptons were treated on equal footing by constructing them from vector-type currents γ^μ. An important step forward from this *Fermi model* of the beta decay, named after its inventor, Enrico Fermi, was taken after the discovery of parity violation. To account for the violation of parity conservation an axial-vector component $\gamma^5\gamma^\mu$ had to be added to the pure vector current, i.e. γ^μ is replaced by a combination $\gamma^\mu(1-\gamma^5)$. The consequence of this *vector minus axial-vector* (V-A) structure is the right-handedness of the electron anti-neutrino in beta-minus decay [20]. The corresponding electron is always left-handed, and the opposite configuration is never allowed.

When the decay process is described by the Feynmann graph of Fig. 2.1, and the V-A structure of the weak currents is taken into account, the

invariant amplitude of the beta-minus decay is written as

$$\mathfrak{M}_{\beta^-} = \left[\frac{g}{\sqrt{2}}\bar{u}_p\gamma^\mu\frac{1}{2}(1-\gamma^5)u_n\right]\frac{1}{M_W^2 - p_W^2}\left[\frac{g}{\sqrt{2}}\bar{u}_e\gamma_\mu\frac{1}{2}(1-\gamma^5)u_{\bar{\nu}_e}\right]. \quad (2.1)$$

The quantities M_W and p_W are mass and momentum of the gauge boson W^-, respectively. The quantity $g/\sqrt{2}$ is used to denote the coupling constants of the weak-interaction vertices.

The Feynman graph of Fig. 2.1, as well as the invariant amplitude of Eq. (2.1), describe a decay process with two interaction vertices. However, due to the large mass of the gauge boson W ($\approx 80\,\mathrm{GeV/c^2}$), this particle decays in a time scale of 10^{-25} s. This represents an extremely narrow time window, and thus the distance propagated by the gauge boson is short even compared to the size of a single nucleon.

Since the energy release of any beta decay is typically less than few MeV, we have $p_W^2 \ll M_W^2$, and Eq. (2.1) then becomes

$$\mathfrak{M}_{\beta^-} = \frac{G_F}{\sqrt{2}}\Big[\bar{u}_p\gamma^\mu(1-\gamma^5)u_n(x)\Big]\Big[\bar{u}_e\gamma_\mu(1-\gamma^5)u_{\bar{\nu}_e}\Big]. \quad (2.2)$$

The new coupling constant G_F of Eq. (2.2) is called the *Fermi coupling constant*, and it is defined as

$$\frac{G_F}{\sqrt{2}} = \frac{g^2}{8M_W^2}. \quad (2.3)$$

The removal of the gauge-boson propagator between the two weak-interaction vertices leads effectively to a point-like interaction. This structure is universal also for other low-energy weak interaction processes [20, 16].

2.2 Renormalization of the hadron current

The V-A structure of the weak currents in Eq. (2.2) leads to a maximal violation of parity due to the equal mixture of vector and axial-vector components. This composition is well-suited for the Dirac leptons. The hadrons, on the other hand, are constructed from individual quarks which in turn are surrounded by a cloud of mesons. Due to the necessity to take into account these additional complexities the hadron current has to be renormalized[2]:

$$\mathfrak{M}_{\beta^-} = \frac{G_F}{\sqrt{2}}\Big[\bar{u}_p\gamma^\mu(g_\mathrm{V} - g_\mathrm{A}\gamma^5)u_n(x)\Big]\Big[\bar{u}_e\gamma_\mu(1-\gamma^5)u_{\bar{\nu}_e}\Big]. \quad (2.4)$$

[2]Note that in many references (including Ref. [16]) the hadron current is renormalized as $\gamma^\mu(1-\lambda\gamma^5)$, where $\lambda = g_\mathrm{A}/g_\mathrm{V}$.

Instead of an equal mixture of vector and axial-vector components, the vector and axial-vector parts of the hadron current in Eq. (2.4) are multiplied by constants g_{V} and g_{A}. These constants are called the vector (V) and axial-vector (A) coupling constants of the weak interaction.

The 'canonical' values of the weak coupling constants are $g_{\mathrm{V}} = 1$ and $g_{\mathrm{A}} = 1.27$ [21]. The unity value of g_{V} is derived from the conserved vector current (CVC) hypothesis of the standard model, and that of g_{A} from the partially conserved axial-vector current (PCAC) hypothesis of the standard model [18]. Both of these values are extracted from the decay of free neutron. Hence, they are also called the 'bare nucleon' values. The CVC hypothesis states that the vector currents $(\bar{\psi}_p \gamma^\mu \psi_n)$ and $(\bar{\psi}_n \gamma^\mu \psi_p)$ form an isospin triplet with the electromagnetic current $(\psi_p \gamma^\mu \psi_p)$ [20]. The connection to the electromagnetic current is thought to protect the vector currents inside the nuclear matter by similar means as the symmetries of the electromagnetic current give rise to the conservation of the electric charge.

Attempts to probe the value of g_{A} by means of practical nuclear-structure calculations (see the discussion in Sect. 3.4) have lead to suggest that some adjustment of the bare nucleon value is needed when working inside the nuclear matter. Part of this quenching can be explained by the non-nucleonic degrees of freedom (see Refs. [18, 22]). However, due to the shortcomings stemming from the nuclear many-body effects (Refs. [23, 24]), the truncations of the model space and/or the deficiencies in the treatment of the many-body quantum mechanics are also absorbed into this constant.

2.3 General theory of beta decay

The general theoretical formalism for the nuclear beta decay is described in great detail in the book by Behrens and Bühring in Ref. [16]. The following overview follows closely that discussion. This section complements the discussion of Ref. [2] that focused on the practical applications of the theory without much insight into the underlying basis of the framework.

To derive a general expression for the beta-decay partial half-life, one must first begin by writing the scattering matrix, or S-matrix. The S-matrix also includes the probability of no interaction among the participating particles. This end-result can be eliminated by defining the so called transition matrix, T-matrix, through

$$S_{fi} = \delta_{fi} + i(2\pi)^4 \delta^4(p_f - p_i) N T_{fi}. \tag{2.5}$$

The function $\delta(p)$ of Eq. (2.5) is the four-dimensional delta function, and N is a normalization factor dependent on the number of initial- and final-state particles.

Starting from the Hamiltonian density

$$H(x) = -\frac{G_\beta}{\sqrt{2}}\{\bar{\psi}_p(x)\gamma_\mu(g_\mathrm{V} - g_\mathrm{A}\gamma_5)\psi_n(x)\bar{\psi}_e(x)\gamma_\mu(1-\gamma_5)\psi_{\nu_e}(x) + h.c.\}, \quad (2.6)$$

where $G_\beta = G_F\cos(\Theta)$ with Θ being the Gabibbo angle, and following the definition of Eq. (2.5), the T-matrix of the beta-minus decay can be expressed as

$$T = -\frac{G_\beta}{\sqrt{2}}\int \langle f|\, V_\mu(0) - A_\mu(0)\,|i\rangle L_\mu(\mathbf{q})\mathrm{d}^3q. \quad (2.7)$$

Since the explicit form of the nuclear current is not known due to the nuclear uncertainties, it is already substituted in Eq. (2.7) by

$$\begin{aligned} i\langle\bar{\psi}_p(x)\gamma_\mu(1-\lambda\gamma_5)\psi_n(x)\rangle &\rightarrow \langle f|\, V_\mu(x) - A_\mu(x)\,|i\rangle \\ &= e^{i(p_i-p_f)x}\langle f|\, V_\mu(0) - A_\mu(0)\,|i\rangle, \end{aligned} \quad (2.8)$$

where V_μ and A_μ denote the vector and axial-vector currents, respectively, and $|i\rangle$ presents the initial and $|f\rangle$ the final nuclear state. The latter form of Eq. (2.8) follows from translational invariance, where p is the total momentum operator.

The function $L_\mu(\mathbf{q})$ of Eq. (2.7) is the Fourier transform of the lepton current, i.e.

$$L_\mu(\mathbf{q}) = \frac{1}{(2\pi)^3}\int e^{-i\mathbf{q}\cdot\mathbf{r}} i\,\bar{u}_e e^{-i\mathbf{p}_e\cdot\mathbf{r}}\,\gamma_\mu(1-\gamma_5)\,v_\nu e^{-i\mathbf{p}_\nu\cdot\mathbf{r}}\,\mathrm{d}^3r, \quad (2.9)$$

where the quantity $\mathbf{q} = \mathbf{p}_f - \mathbf{p}_i = -(\mathbf{p}_e + \mathbf{p}_\nu)$ is the momentum transfer. The lepton part of the T-matrix can then be treated by inserting the plane-wave expansion

$$e^{i\mathbf{q}\cdot\mathbf{r}} = 4\pi\sum_{LM} i^L j_L(qr)Y_L^{*M}(\hat{q})Y_L^M(\hat{r}) \quad (2.10)$$

in Eq. (2.9). The functions j_L and Y_L^M are the Bessel function and the spherical harmonics, respectively.

To treat the hadron part of Eq. (2.7) a more careful analysis is needed to derive usable expressions for the practical application of the theory. A crucial step in overcoming these complications is to divide the nuclear current into space and time components, and then expand them through the multipole

decomposition (here Ref. [16] points out another reference by Stech and Schülke [25]):

$$\langle f|\, V_0(0)+A_0(0)\,|i\rangle = \sum_{LM}(-1)^{J_f-M_f}\sqrt{2J_f+1} \times \begin{pmatrix} J_f & L & J_i \\ -M_f & M & M_i \end{pmatrix} \sqrt{4\pi}\, Y_L^{*M}(\hat{q})\frac{(qR)^L}{(2L+1)!!}F_L(q^2) \tag{2.11a}$$

$$\langle f|\, \mathbf{V}(0)+\mathbf{A}(0)\,|i\rangle = \sum_{KLM}(-1)^{J_f-M_f}\sqrt{2J_f+1} \times \begin{pmatrix} J_f & K & J_i \\ -M_f & M & M_i \end{pmatrix} \sqrt{4\pi}\, \mathbf{Y}_{KL}^{*M}(\hat{q})\frac{(qR)^L}{(2L+1)!!}F_{KL}(q^2). \tag{2.11b}$$

The form factors $F_L(q^2)$ and $F_{KL}(q^2)$ of Eq. (2.11) act as reduced matrix elements that describe a transition between two nuclei with a relative momentum $q = |\mathbf{q}|$ and a relative angular momentum L. The total angular momentum K of the factor $F_{KL}(q^2)$ is the angular momentum L coupled with the vector operator $\boldsymbol{\sigma}$ or $\mathbf{p}$. The quantity R is the nuclear radius.

The functions Y_L^{*M} and $\mathbf{Y}_{KL}^{*M}$ of Eq. (2.11), related to the momentum transfer q, are the spherical harmonics and vector spherical harmonics, respectively. These can be used to define an irreducible tensor operator T_{KLs}^M written as

$$T_{LL0}^M(\hat{q}) = i^L Y_L^M(\hat{q}) \tag{2.12a}$$

$$T_{KL1}^M(\hat{q}) = (-1)^{L-K+1} i^L \mathbf{Y}_{KL}^M(\hat{q})\cdot\alpha = \sum_{\mu} C(1\,L\,K;\,\mu\,M-\mu) i^L \gamma_5 \sigma_\mu Y_L^{M-\mu}(\hat{q}), \tag{2.12b}$$

where the quantities $C(l_1\,l_2\,j;\,m_1\,m_2)$ are the Clebsch-Gordan coefficients. By using the tensor operator T_{KLs}^M the decompositions of Eq. (2.11) can be combined into a single equation:

$$(-i)\langle f|\, V_\mu(0)+A_\mu(0)\,|i\rangle\gamma_4\gamma_\mu = \sum_{KLMs}(-1)^{J_f-M_f+M}(-i)^L\sqrt{4\pi}\sqrt{2J_i+1} \times \begin{pmatrix} J_f & K & J_i \\ -M_f & M & M_i \end{pmatrix} T_{KLs}^{-M}(\hat{q})\,\frac{(qR)^L}{(2L+1)!!}\,F_{KLs}(q^2). \tag{2.13}$$

The old form factors F_L and F_{KL} of Eq. (2.11) are related to F_{KLs} by

$$F_{KLs} = \begin{cases} F_L\delta_{KL} & \text{for } s=0 \\ F_{KL} & \text{for } s=1. \end{cases} \tag{2.14}$$

It should be noted that $\gamma_4\gamma_\mu$ is taken from the lepton matrix element. Therefore the tensor operator T^M_{KLs} acts on the lepton spinors.

The treatment of the lepton part is further aided by the introduction of a spherical basis for the lepton wave functions. Thus, by applying a partial wave expansion $\phi(\mathbf{r}) = \sum_{\kappa\mu} a_{\kappa\mu}\phi^\mu_\kappa$ to the electron and neutrino wave functions (see the details e.g. in Ref. [16]), the corresponding spherical waves are given by

$$\phi^\mu_\kappa(\mathbf{r}) = \begin{pmatrix} \mathrm{sign}(\kappa) f_\kappa(r)\chi^\mu_{-\kappa}(\mathbf{r}) \\ g_\kappa(r)\chi^\mu_\kappa(\mathbf{r}) \end{pmatrix}, \tag{2.15}$$

where

$$\chi^\mu_\kappa(\mathbf{r}) = i^l \sum_m C(l\,1/2\,j;\,\mu - m\,m) Y_l^{\mu-m}(\mathbf{r})\chi^m. \tag{2.16}$$

The two-component spinor χ^m is the Pauli spinor, and the adopted sign convention for the radial function (2.15) is taken to be

$$\mathrm{sign}(\kappa) = (-1)^{j-l+1/2}. \tag{2.17}$$

The index κ, related to the values l and j of the orbital and total angular momentum of the lepton, is defined as follows:

$$\kappa = \begin{cases} l & \text{for } \; j = l - 1/2 \\ -(l+1) & \text{for } \; j = l + 1/2. \end{cases} \tag{2.18}$$

The general expressions for the radial functions $g_\kappa(r)$ and $f_\kappa(r)$ of the spherical lepton waves are given by

$$g_\kappa(r) = \sqrt{\frac{W+m}{W}} j_l(pr) \tag{2.19a}$$

$$f_\kappa(r) = \mathrm{sign}(\kappa)\sqrt{\frac{W-m}{W}} j_{\bar{l}}(pr). \tag{2.19b}$$

The quantity m is the lepton rest mass, and $\bar{l}$ denotes the values $l(\kappa) - 1$ for $\kappa > 0$ and $l(\kappa) + 1$ for $\kappa < 0$. The coefficients $a_{\kappa\mu}$ of the spherical-wave expansion are taken from

$$a_{\kappa\mu} = \frac{4\pi}{\sqrt{2}} C(l\,1/2\,j;\,\mu - m\,m) Y_l^{*\,\mu-m}(\hat{p}). \tag{2.20}$$

In order to assure the desired asymptotic behaviour for $r \to \infty$ (check the details in Ref. [16]), the radial functions of the electron are usually multiplied by the electron momentum p_e. With this choice the corresponding quantities $a_{\kappa\mu}$ need to be divided by p_e.

It should be noted that the rest mass of the neutrino is usually assumed to be zero when writing the radial functions of Eq. (2.19). This contradicts the current understanding about the properties of neutrinos, but in practice the effects stemming from this simplification are negligible for most beta decays. Essentially, the finite rest-mass of the neutrino has any significance only for decays with ultra-low Q-values.

By adding Eqs. (2.9) and (2.11) together, the T-matrix of Eq. (2.7) can be written as

$$\begin{aligned} T_{\beta-} =& \frac{G_\beta}{\sqrt{2}} \frac{1}{\pi^{3/2}} \sum_{KLMs} \sum_{\kappa_e \mu_e \kappa_\nu \mu_\nu} (-1)^{J_f - M_f + j_e - \mu_e} (-1)^{L+M+j_\nu+\mu_\nu} \\ & \times \sqrt{2J_i+1} \begin{pmatrix} J_f & K & J_i \\ -M_f & M & M_i \end{pmatrix} \begin{pmatrix} j_e & K & j_\nu \\ -\mu_e & -M & -\mu_\nu \end{pmatrix} \\ & \times a^*_{\kappa_e \mu_e} a^*_{\kappa_\nu \mu_\nu} \int_0^\infty q^2 \mathrm{d}q \int_0^\infty r^2 \mathrm{d}r \frac{(qR)^L}{(2L+1)!!} j_L(qr) F_{KLs}(q^2) \\ & \times \langle \phi_{\kappa_e} || T_{KLs}(1+\gamma_5) \, || \phi_{\kappa_\nu} \rangle. \end{aligned} \tag{2.21}$$

When the rest-mass of the emitted (anti-)neutrino is assumed to be zero, the lepton matrix element is expressed as

$$\begin{aligned} \langle \phi_{\kappa_e} | T_{KLs}(1+\gamma_5) \, | \phi_{\kappa_\nu} \rangle =& \, g_{\kappa_e}(-Z) \{ j_{l(\kappa_\nu)}(p_\nu r) G_{KLs}(\kappa_e, -\kappa_\nu) \\ & + j_{l(-\kappa_\nu)}(p_\nu r) G_{KLs}(\kappa_e, \kappa_\nu) - \mathrm{sign}(\kappa_e) j_{l(\kappa_\nu)}(p_\nu r) G_{KLs}(-\kappa_e, \kappa_\nu) \\ & + j_{l(-\kappa_\nu)}(p_\nu r) G_{KLs}(-\kappa_e, -\kappa_\nu) \}. \end{aligned} \tag{2.22}$$

The explicit expression for G_{KLs} is given by

$$\begin{aligned} G_{KLs}(\kappa_e, \kappa_\nu) =& \, i^{l_e + l_\nu + L} (-1)^{j_e - j_\nu} \\ & \times \sqrt{(2s+1)(2K+1)(2j_e+1)(2j_\nu+1)(2l_e+1)(2l_\nu+1)} \\ & \times C(l_e \, l_\nu \, L; \, 0 \, 0) \begin{Bmatrix} K & s & L \\ j_e & 1/2 & l_e \\ j_\nu & 1/2 & l_\nu \end{Bmatrix}. \end{aligned} \tag{2.23}$$

To simplify the above expressions for a more convenient application of the theory, the integral of Eq. (2.21) is abbreviated as

$$\begin{aligned} & \frac{2}{\pi} \frac{1}{\sqrt{2K+1}} \sum_{Ls} (-1)^{K-L} \int_0^\infty q^2 \mathrm{d}q \int_0^\infty r^2 \mathrm{d}r \frac{(qR)^L}{(2L+1)!!} j_L(qr) F_{KLs}(q^2) \\ & \quad \times \{ g_{\kappa_e}(r) [j_l(p_\nu r) G_{KLs}(\kappa_e, \kappa_\nu) - j_{\bar{l}}(p_\nu r) G_{KLs}(\kappa_e, -\kappa_\nu)] \\ & \qquad + \mathrm{sign}(\kappa_e) f_{\kappa_e}(r) [j_l(p_\nu r) G_{KLs}(-\kappa_e, \kappa_\nu) - j_{\bar{l}}(p_\nu r) G_{KLs}(-\kappa_e, -\kappa_\nu)] \} \\ & \quad = -\mathrm{sign}(\kappa_\nu) \alpha_{\kappa_e} \{ M_K(k_e, k_\nu) + \mathrm{sign}(\kappa_e) m_K(k_e, k_\nu) \}, \end{aligned} \tag{2.24}$$

where α_{κ_e} are a set of normalization constants for the electron radial wave functions (see the presentation of the radial functions and the associated normalization constants in Ref. [16]). The functions $M_K(k_e, k_\nu)$ and $m_K(k_e, k_\nu)$ are used to store the nuclear-structure information together with the various other kinematical factors. Thus, the T-matrix can finally be written more compactly as

$$\begin{aligned} T_{\beta-} =& \frac{G_\beta}{4\pi}\frac{1}{\pi^{3/2}}\sum_{KM}\sum_{\kappa_e\mu_e\kappa_\nu\mu_\nu}(-1)^{J_f-M_f+K+M+j_e-\mu_e+\mu_\nu-l_\nu+1/2} \\ & \times \sqrt{(2J_i+1)(2K+1)}\begin{pmatrix} J_f & K & J_i \\ -M_f & M & M_i \end{pmatrix}\begin{pmatrix} j_e & K & j_\nu \\ -\mu_e & -M & -\mu_\nu \end{pmatrix} \\ & \times a^*_{\kappa_e\mu_e}a^*_{\kappa_\nu\mu_\nu}\alpha_{\kappa_e}\left\{M_K(k_e,k_\nu)+\mathrm{sign}(\kappa_e)m_K(k_e,k_\nu)\right\}. \end{aligned} \tag{2.25}$$

Using the T-matrix of Eq. (2.25) the probability for a beta particle to be emitted in an energy interval from W_e to $W_e + \mathrm{d}W_e$ is given by

$$P(W_e)\mathrm{d}W_e = \frac{\sum_f\sum_s |T|^2}{2\pi^2}p_eW_e(W_0-W_e)^2\mathrm{d}W_e, \tag{2.26}$$

where universal factor $p_eW_e(W_0 - W_e)^2$ is the statistical energy distribution of the beta particle which follows from the density of final states. Deviations from the statistical shape are included into the T-matrix. These deviations result from the properties of nuclear structure and from the coulomb interaction between the decay remnants.

2.4 The leading-order and next-to-leading-order terms of the beta-decay shape factor

When only the beta spectrum, and no neutrino, is observed one must integrate over the direction of the emitted beta particle. Furthermore, if the transition proceeds via non-orientated initial and final nuclear states, one must also average over the initial substates M_i and sum over the final substates M_f. In that case the beta spectrum of Eq. (2.26) can be simplified further and expressed as

$$P(W_e)\mathrm{d}W_e = \frac{G_F^2}{2\pi^3}C(W_e)\,p_eW_e(W_0-W_e)^2\,F_0(Z,W_e)\mathrm{d}W_e. \tag{2.27}$$

The function $F_0(Z, W_e)$ of Eq. (2.27) is the Fermi function, and it approximately takes into account the coulombic interaction between the beta particle and the daughter nucleus. The nuclear-structure information, previously

stored inside the T-matrix, is now included into the shape factor $C(W_e)$ given by

$$C(W_e) = \sum_{k_e k_\nu K} \lambda_{k_e} \Bigg\{ M_{\mathrm{K}}^2(k_e, k_\nu) + m_{\mathrm{K}}^2(k_e, k_\nu) - \frac{2\mu_{k_e}\gamma_{k_e}}{k_e W_e} M_{\mathrm{K}}(k_e, k_\nu) m_{\mathrm{K}}(k_e, k_\nu) \Bigg\}, \tag{2.28}$$

where λ_{k_e} and μ_{k_e} are the beta-decay coulomb functions. Typically (see Ref. [16]), it is assumed that $\mu_{k_e} \approx 1$, and λ_{k_e} is taken to be

$$\lambda_{k_e} = \frac{F_{k_e-1}(Z, W_e)}{F_0(Z, W_e)}. \tag{2.29}$$

The function $F_{k_e-1}(Z, W_e)$ is called the generalized Fermi function (see the explicit expression e.g. in Ref. [2]). The quantity $\gamma_{k_e} = \sqrt{k_e^2 - (\alpha Z)^2}$, where α is the fine-structure constant and Z the proton number of the daughter nucleus.

The decay rate of a beta decay transition is determined by simply integrating Eq. (2.27) over the electron energies, i.e.

$$\lambda = \int_{m_e c^2}^{W_0} P(W_e) \mathrm{d}W_e. \tag{2.30}$$

The upper limit W_0 of the integral, called the end-point energy, corresponds to the maximum electron (positron) energy. The partial half-life of the decay branch is derived from the decay rate by $t_{1/2} = \ln 2/\lambda$.

Due to the complexity of the functions $M_K(k_e, k_\nu)$ and $m_K(k_e, k_\nu)$ in Eq. (2.28), any practical calculations of the beta decay observables are performed by concentrating only on the most significant contributions of the shape factor. When the form factors $F_{KLs}(q^2)$ of Eq. (2.11) are expressed in terms of the *form-factor coefficients* F_{KLs}^N (see Ref. [16]), the leading contributions come essentially from the few lowest non-zero coefficients that correspond to the least angular-momentum transfer between the initial and final nuclear states. Further simplification can, however, be attained due to the suppression stemming from the small quantities αZ, $p_e R/\hbar$, $qR/\hbar$, $m_e cR/\hbar$ and $W_e R/\hbar c$. Since various combinations of these quantities appear as prefactors of the form-factor coefficients, the contributions of the form-factor terms can be arranged according to the powers of the small quantities involved (see details in Refs. [1, 2]).

Following the order-of-magnitude considerations outlined e.g. in Refs. [16, 17], the theoretical computations are typically performed using only the

Table 2.2: The leading-order and next-to-leading-order nuclear matrix elements of beta decay. Note that k_e takes integer values between 1 and K, where K is the level of forbiddenness of the transition.

	Vector (V)	Axial-vector (A)
Leading order	${}^{V}M^{(0)}_{KK-11}$ ${}^{V}M^{(0)}_{KK0}$ ${}^{V}M^{(0)}_{KK0}(k_e,1,1,1)$	${}^{A}M^{(0)}_{KK1}$ ${}^{A}M^{(0)}_{KK1}(k_e,1,1,1)$ ${}^{A}M^{(0)}_{K+1K1}$ ${}^{A}M^{(0)}_{000}$ ${}^{A}M^{(0)}_{011}$ ${}^{A}M^{(0)}_{011}(k_e,1,1,1)$
Next-to-leading order	${}^{V}M^{(1)}_{KK-11}$ ${}^{V}M^{(1)}_{KK-11}(k_e,1,1,1)$ ${}^{V}M^{(1)}_{KK-11}(k_e,2,1,1)$ ${}^{V}M^{(1)}_{KK-11}(k_e,2,2,1)$ ${}^{V}M^{(1)}_{KK-11}(k_e,2,2,2)$ ${}^{V}M^{(0)}_{KK+11}$ ${}^{V}M^{(0)}_{KK+11}(k_e,1,1,1)$ ${}^{V}M^{(0)}_{K+1K+11}$ ${}^{V}M^{(0)}_{K+1K+11}(k_e,1,1,1)$	${}^{A}M^{(1)}_{KK1}$ ${}^{A}M^{(0)}_{K+1K+10}$ ${}^{A}M^{(0)}_{K+1K+10}(k_e,1,1,1)$

leading-order contributions (check e.g. Refs. [13, 12]). In Refs. [1, 2] the theoretical formalism is expanded to the next-to-leading order. When the next-to-leading-order terms of the shape factor are included, the number of nuclear matrix elements increases from $2K+4$ to $9K+9$ for non-unique decays, where K is the level of forbiddenness of the transition. A summary of these elements is presented in Table 2.2. The explicit expression are given in Ref. [2]. Note that the matrix elements ${}^{A}M^{(0)}_{000}$, ${}^{A}M^{(0)}_{011}$ and ${}^{A}M^{(0)}_{011}(k_e,1,1,1)$ are non-zero only for the first-forbidden decays with $\Delta J = 0$.

3 Application and results

The theoretical description of rare beta decays is demanding due to the low Q-values and/or high levels of forbiddenness. Low Q-values give rise to additional effects that are typically neglected for the more usual type of transitions. High forbiddenness, on the other hand, amounts to a drastic increase in the number of nuclear matrix elements.

Low energy release, i.e. low Q-value, gives rise to a small transition phase space. This, in return, leads to long partial half-lives. The interest towards the nuclear single beta decays with ultra-low Q-values is mainly explained by their application to experiments aiming to determine the mass of neutrino. Although a lot of information about the relative masses and mixing of neutrinos exists to date, the absolute mass scale remains unknown.

The partial half-lives of highly-forbidden transition are similarly long. This is due to the reduced probability of emitting a lepton pair which has a large enough angular momentum to overcome the angular-momentum difference between the initial and final nuclear states. Valuable information on such decays can thus be achieved using theoretical frameworks to estimate their partial half-lives and beta spectra. As a highlight of this thesis an overview of the application of the spectrum-shape method (SSM) is also made. This method was recently developed for the extraction of the effective values of the weak coupling constants.

3.1 The possible ultra-low Q-value branch of ^{115}Cd

The experiments that utilize single beta decays to probe the neutrino rest-mass are focused on the high-precision measurements of beta-particle spectra. In the presence of a neutrino with non-zero rest-mass an equal amount of offset is introduced to the value of the end-point energy. More notably, however, the spectrum is also distorted near the end-point region. For non-zero neutrino rest-mass the slope of the end-point spectrum is infinite rather than zero. To detect this slight distortion, Q-values as low as possible are desirable.

The studies on beta particle spectra are currently used to determine the electron-neutrino rest-mass in the KATRIN (see Ref. [10]) and MARE (Ref.

[11]) experiments. These experiments concern the use of tritium ($Q = 18.592$ keV $\pm < 0.5$ eV [26]) and ^{187}Re ($Q = 2.467(2)$ keV [26]), respectively, as beta-particle sources. Since the need for low Q-values is a highly limiting requirement for the sources, the search for suitable decays continues. Recently a suitable ultra-low-Q-value candidate for the neutrino studies was identified in the nucleus ^{115}In. There the $9/2^+$ ground state decays to the first excited state $3/2^+$ of ^{115}Sn with a world-record small Q-value of (0.173 ± 0.012) keV [27, 28]. Up to date, the partial half-life of this decay branch is most accurately measured to be $(4.3\pm0.5)\cdot10^{20}$ yr in Ref. [29] (note that partial half-life quoted in Ref. [12] was taken from a slightly older study found in Ref. [30]). Another potential ultra-low-Q-value decay branch can be identified in ^{135}Cs (see Ref. [31]), but the Q-value is not resolved experimentally.

While the studies on single beta decay are direct searches of the electron-neutrino mass, experiments that focus on the double beta decay are indirect. Such experiments involve the measurement of the effective (Majorana) neutrino mass, and are highly sensitive to the uncertainties of the nuclear matrix elements [5, 32, 33].

Aside from the attempts the explore the neutrino rest-mass, the studies on ultra-low-Q-value beta decays can also increase our understanding on the atomic effects that are usually neglected in decays with higher energy release. These effects include the screening of atomic electrons, mismatch between the initial and final atomic states, the atomic exchange effects as well as the influence of the molecular or lattice structure. Since only few studies exist (see e.g. Refs. [34, 35]) very little is known about these effects in general.

In Ref. [12] nuclear-model calculations with the microscopic quasiparticle-phonon model (MQPM) were used to analyse the various beta-decay branches of ^{115}Cd (see Fig. 3.1), and to test the performance of the nuclear model itself. Due to the isomeric nature of the first excited state, $11/2^-_1$, both the ground state and the first excited state can decay via beta decay. Among the many available decay channels there exists also a possible ultra-low-Q-value branch $1/2^+_{\text{g.s.}} \rightarrow 9/2^+_3$ which is a fourth-forbidden transition. The Q-value (-2.8 ± 4.0) keV of this transition is derived from the ground-state-to-ground-state Q-value (1446 ± 4) keV [36], but accurate measurements, e.g. with Penning-trap techniques (see e.g. Ref. [27]), are needed to verify the precise value, and thus to judge the detectability of this decay branch.

The MQPM framework is well-suited to nuclear-structure studies of spherical or nearly spherical odd-A medium-heavy nuclei with open-shell configurations [37]. Details of the present MQPM calculations of the nuclei ^{115}Cd and ^{115}In are summarized in Ref. [12]. Other applications of the framework can be found e.g. in Refs. [1, 2, 13], where the framework was applied to the

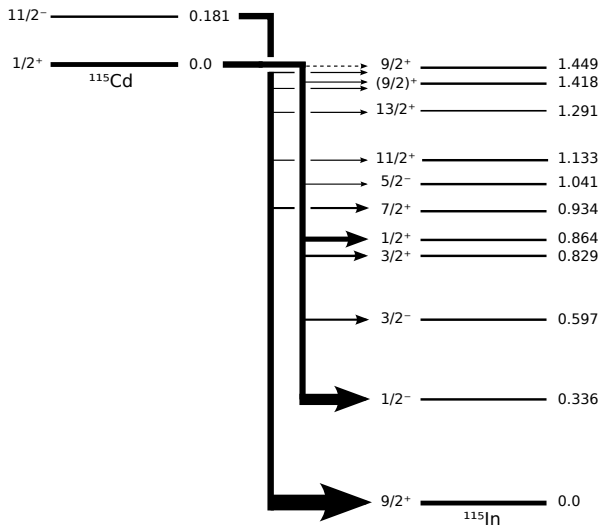

Figure 3.1: Beta-decay branches of ^{115}Cd. Both the ground state and the isomeric first excited state of ^{115}Cd decay via beta decay. The ultra-low-Q-value decay branch is indicated by a dashed line.

beta decays of ^{113}Cd and ^{115}In. A very recent and more extensive application was carried out in Ref. [19], where a total of 26 beta-decay transitions was studied using this nuclear model. The proton-neutron variant of MQPM, i.e. the pnMQPM, for odd-odd nuclei is presented in Ref. [38].

Since there exists no experimentally measured Q-value for the $1/2^+_{\text{g.s.}} \rightarrow 9/2^+_3$ transition, the partial half-life of this decay branch is presented as a function of the Q-value in Fig. 3.2. Based on the different fits of the underlying QRPA phonons (see details in Ref. [12]) a band of theoretical partial half-life values is presented as a dark-shaded area. Due to the fact that most of the uncertainties can be expected to be associated to the wave function of the $9/2^+_3$ state, and that the transition $11/2^-_1 \rightarrow 9/2^+_3$ was found to be an order of magnitude too fast (see Table 3.1), a systematic error, represented by the light-shaded area in the figure, was assigned to the calculations. This corresponds to a factor of 10 increase to the computed theoretical value. It should further be noted that only the first-order terms of the beta-decay shape factor were used to calculate the partial half-life.

In general, the results of Table 3.1 show a fairly satisfactory agreement with the experimental data considering that the various decay branches span a huge range of partial-half-life values. Deviations from the experiment can, at least to a certain degree, be associated with the omission of the

Table 3.1: Computed partial half-lives for the various beta-decay branches of ^{115}Cd. Tabulation excludes the ultra-low-Q-value branch that is presented in Fig. 3.2. No experimental partial half-life is available for the $1/2^+_{\text{g.s.}} \rightarrow 9/2^+_2$ branch.

Initial state $(J^\pi)_i = 1/2^+_{\text{g.s.}}$ (0.0 MeV)				
$(J^\pi)_f$	Q (MeV)	$t^{(\text{exp.})}_{1/2}$	Theoretical partial half-life	
			$g_{\text{A}} = 1.25$	$g_{\text{A}} = 1.00$
$1/2^-_1$	1.1097	3.56 d	(3.9 ± 0.3) d	(6.1 ± 0.6) d
$3/2^-_1$	0.8486	192.03 d	(1.28 ± 0.09) d	(1.48 ± 0.11) d
$3/2^+_1$	0.6174	67.50 d	(10.9 ± 0.4) h	(17.1 ± 0.7) h
$1/2^+_1$	0.5819	6.73 d	(1.84 ± 0.06) h	(2.85 ± 0.10) h
$5/2^-_1$	0.4046	7628.42 yr	(3000 ± 400) yr	(4700 ± 600) yr
$9/2^+_2$	0.0277	-	$(1.0 \pm 0.3) \times 10^{25}$ yr	$(1.5 \pm 0.5) \times 10^{24}$ yr
Initial state $(J^\pi)_i = 11/2^-_1$ (0.181 MeV)				
$(J^\pi)_f$	Q (MeV)	$t^{(\text{exp.})}_{1/2}$	Theoretical partial half-life	
			$g_{\text{A}} = 1.25$	$g_{\text{A}} = 1.00$
$9/2^+_{\text{g.s.}}$	1.6270	45.94 d	(3.0 ± 0.3) h	(2.3 ± 0.2) h
$7/2^+_1$	0.6932	7.18 yr	(1100 ± 400) yr	(1800 ± 500) yr
$11/2^+_1$	0.4944	203.47 yr	(90 ± 50) yr	(90 ± 50) yr
$13/2^+_1$	0.3364	13.56 yr	(25 ± 4) yr	(26 ± 4) yr
$9/2^+_2$	0.2087	40.69 yr	(40 ± 30) yr	(30 ± 20) yr
$9/2^+_3$	0.1782	610.41 yr	(60 ± 50) yr	(50 ± 40) yr

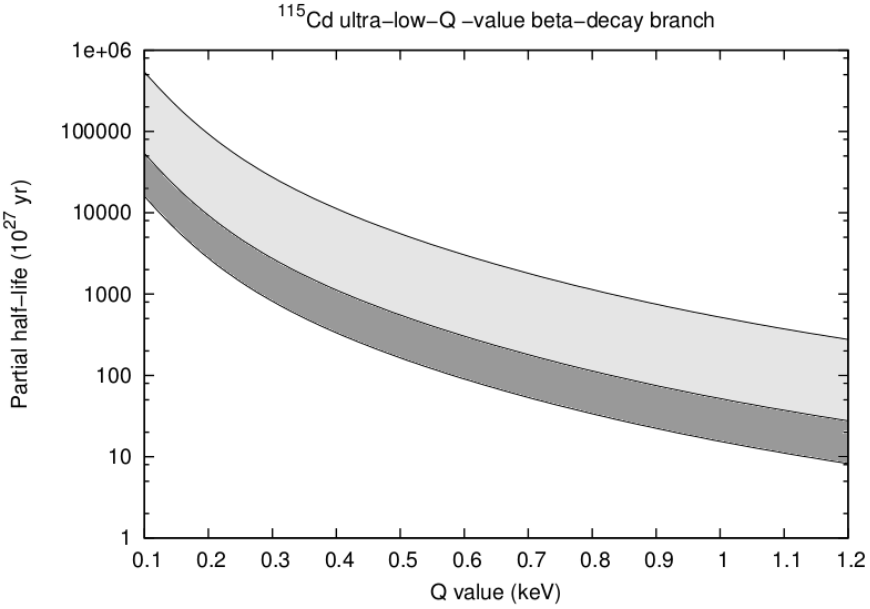

Figure 3.2: Partial half-life of the ultra-low-Q-value beta-decay branch of ^{115}Cd as a function of the Q-value.

five-quasiparticle degrees of freedom. These effects are beyond the MQPM framework since the wave functions are constructed from one- and three-quasiparticle components.

3.2 Highly-forbidden beta-decay channels of ^{48}Ca and ^{50}V

The two unstable nuclei ^{48}Ca and ^{50}V share a similar feature. That is, the long half-life is attributed to the unfavourable nuclear structure mismatch between the initial and final state nuclei. Consequently, in both cases the available single beta decay channel is also overcome by a more competing decay process. For ^{50}V the stronger decay channel is the electron capture (EC). For the ^{48}Ca, however, this channel is the double beta decay.

In contrast to the large number of isotopes across the nuclear landscape that decay via nuclear single beta decay, there exist much less verified candidates of nuclear double beta decay. For two candidates, namely ^{48}Ca (see Refs. [14, 39, 40, 41, 42, 43, 44]) and ^{96}Zr (Refs. [15, 45, 46]), the two-neutrino mode of double beta decay competes with single beta decay. In

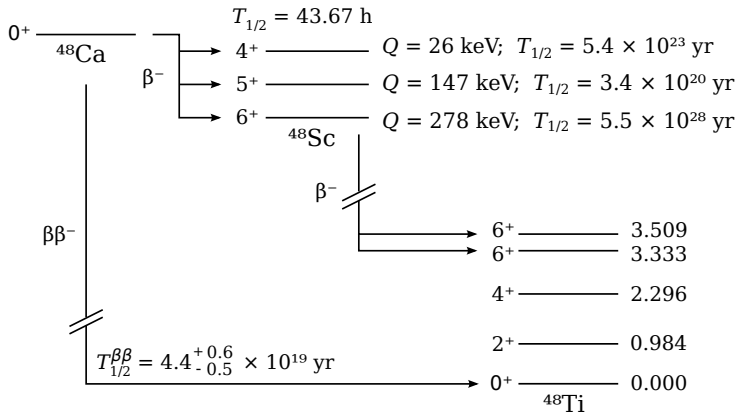

Figure 3.3: Computed single and experimental double beta-decay half-lives of ^{48}Ca.

both cases the single beta decay is suppressed by a high level of forbiddeness. Currently the most up-to-date half-life of the $2\nu\beta\beta$ channel is analysed to be $T^{2\nu}_{1/2} = (4.4^{+0.6}_{-0.5}) \times 10^{19}$ yr for ^{48}Ca, and $T^{2\nu}_{1/2} = (2.3 \pm 0.2) \times 10^{19}$ yr for ^{96}Zr [42].

In Ref. [3] the single beta decay channels of the double magic ^{48}Ca were examined using the nuclear shell model (NSM) (see e.g. Refs. [14, 47, 48]). The one-body transition densities (OBTDs) were calculated for the full pf shell using the GXPF1A interaction [49, 50]. The validity of this interaction in the computation of beta-decay OBTDs has previously been tested e.g. in Refs. [51, 52]. Applications to the computation of double-beta-decay matrix elements of ^{48}Ca have also been performed in Refs. [52, 53, 54]. This includes both the two-neutrino and the neutrinoless modes of double beta decay.

Since the single-beta-decay half-life of ^{48}Ca is not measured and only lower limits of the individual beta branches exist (see Ref. [44]), the competition between the two decay channels was investigated by comparing the computed single-beta-decay partial half-lives with the experimental double-beta-decay half-life. The computed beta-decay half-lives are presented in Fig. 3.3 and Table 3.2. According to the results presented in Table 3.2, the dominant decay branch is the fourth-forbidden unique to the 5^+ final state, leading to the predicted single-beta-decay half-life of $T^{\beta}_{1/2} = (5.2^{+1.7}_{-1.3}) \times 10^{20}\, g_{\rm A}^{-2}$ yr, where $g_{\rm A}$ is the value of the axial-vector coupling constant. This is a factor $2-3$ times longer than the experimental lower limits of the single-beta-decay branches, and approximately 12 times longer than the double-beta-decay half-life.

Table 3.2: Theoretical partial half-lives for the beta-decay branches of ^{48}Ca. Forbiddenness of the transition (K) is presented in the second column. Note that the lower limits quoted in Ref. [3] were taken from Ref. [43].

Transition	K	$t_{1/2}^{(\mathrm{exp.})}$ (10^{20} yr)	Theoretical partial half-life	
			$g_{\mathrm{A}} = 1.25$	$g_{\mathrm{A}} = 1.00$
$0^+_{\mathrm{g.s.}} \to 6^+_{\mathrm{g.s.}}$	6	> 1.6	$(5.46^{+1.18}_{-0.96}) \times 10^{28}$ yr	$(5.18^{+1.11}_{-0.91}) \times 10^{28}$ yr
$0^+_{\mathrm{g.s.}} \to 5^+_1$	4u	> 2.5	$(3.36^{+1.08}_{-0.79}) \times 10^{20}$ yr	$(5.25^{+1.70}_{-1.24}) \times 10^{20}$ yr
$0^+_{\mathrm{g.s.}} \to 4^+_1$	4	> 1.9	$(5.37^{+13.03}_{-3.47}) \times 10^{23}$ yr	$(4.50^{+10.90}_{-2.91}) \times 10^{23}$ yr

The single-beta-decay channels of ^{48}Ca were previously studied in Ref. [14] using NSM-based OBTDs. In that study the single-beta-decay half-life was computed to be $T^{\beta}_{1/2} = (1.1^{+0.8}_{-0.6}) \times 10^{21}\, g_{\mathrm{A}}^{-2}$ yr. When comparing the current theoretical prediction to the previous result, the current single-beta-decay half-life is 53% shorter. This indicates a stronger competition between the two decay channels, but it is not enough to change the final outcome. As a conclusion, the double-beta-decay channel is still relatively weakly challenged by the single-beta-decay. The fact that the single-beta-decay half-life is dominated by the fourth-forbidden unique transition, and not the non-unique one, follows from the smaller Q-value of the 4^+ transition and phase-space considerations that strongly favour unique decays over the non-unique ones.

In Ref. [3] an additional study was made to examine the role of screening of the atomic electrons. To take these effects into account a screening-corrected shape factor (see details in Ref. [55]) was used to calculate the partial half-lives. In beta-minus decay this correction amounts to reduction of the size of the transition phase-space at low energies. As a consequence the higher-energy electrons are favoured and the decay probability is reduced leading to longer partial half-lives. In the current study these corrections were found to be practically negligible. The effect on the partial half-life was less than 1%. This is surprisingly little, and the discrepancy between the present calculations and those of Ref. [47] lends no easy explanation. In Ref. [47] the screening corrections were reported to amount up to 11% effect.

The detectability of the ^{50}V beta-minus decay channel was studied in Ref. [4]. Similarly to the beta decay studies of ^{48}Ca, the OBTDs were calculated using the NSM with the GXPF1A interaction. The decay scheme is presented in Fig. 3.4, including both the EC and the beta-minus decay branches. Since the angular-momentum change in a ground-state-to-ground-state transition would amount to a total of $\Delta J = 6$, the nucleus ^{50}V decays to the 2^+ first

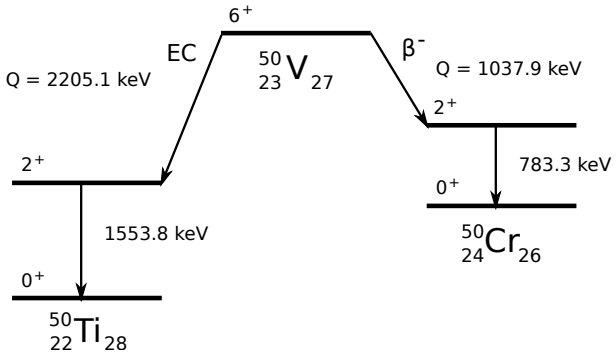

Figure 3.4: The fourth-forbidden non-unique beta-decay and electron-capture channels of ^{50}V.

Table 3.3: Theoretical partial half-lives for the fourth-forbidden non-unique beta-decay branches of ^{50}V.

Transition	$t_{1/2}^{(\mathrm{exp.})}$ (10^{17} yr)	Theoretical partial half-life (10^{17} yr)	
		$g_{\mathrm{A}} = 1.25$	$g_{\mathrm{A}} = 1.00$
$^{50}\mathrm{V}(6^+_{\mathrm{g.s.}}) \rightarrow {}^{50}\mathrm{Ti}(2^+_1)$	2.29 ± 0.25	3.63 ± 0.05	5.13 ± 0.07
$^{50}\mathrm{V}(6^+_{\mathrm{g.s.}}) \rightarrow {}^{50}\mathrm{Cr}(2^+_1)$	> 17	200 ± 2	234 ± 2

excited states in both directions. As in the case of ^{48}Ca, the reduction of the level of forbiddenness from $K = 6$ to $K = 4$ lowers the partial half-lives by several orders of magnitude.

Considerable care was taken to ensure that the spectroscopic properties of ^{50}Ti, ^{50}V and ^{50}Cr are well-reproduced using the NSM calculations (see calculated level schemes, as well as the predicted B(E2) values and the electric quadrupole and magnetic moments in Ref. [4]). As a consequence, a fairly good agreement between the experimental and theoretical partial half-lives of the EC branch can be seen in the results of Table 3.3. The presented theoretical prediction for the beta-decay partial half-life is also seen to agree with the most recent experimental lower limit 1.7×10^{18} yr [56], although it is an order of magnitude longer. Considering that the EC half-life was slightly overshot, the current estimate for the beta-minus decay branch might also indicate a bit too high suppression for the decay probability.

A claimed observation of the single-beta-decay branch of ^{50}V was earlier made in Ref. [57] with a half-life of $t_{1/2}^{\beta^-} = (8.2^{+13.1}_{-3.1}) \times 10^{17}$ yr. The experimentally deduced value of that study is in a tension with the latest lower limit

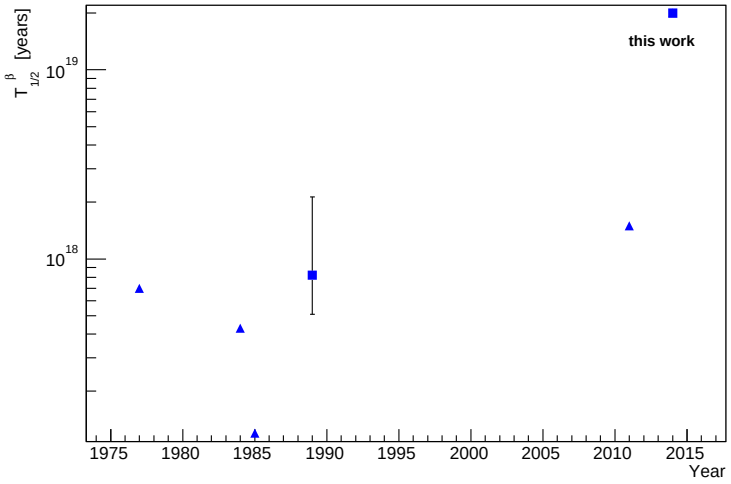

Figure 3.5: Summary of the lower limits of the ^{50}V beta-minus-decay branch. The graph includes the one positive claim made in Ref. [57] and the theoretical estimate computed in Ref. [4].

(see the discussion in Ref. [56]), and it is in a strong conflict with the current theoretical prediction. A comparison between the theoretical estimate and the proposed experimental half-life shows that the theoretical value is 24 times longer.

A summary of the experimental lower limits obtained for the beta-decay partial half-life of ^{50}V, including the one positive claim, can be found in Fig. 3.5. When assessing the experimental detectability of the beta-minus-decay branch in terms of the latest lower limit, a new experiment with an order of magnitude better sensitivity is in order. Details on how the required improvement on the experimental set-up could be achieved is briefly discussed at the end of Ref. [4].

3.3 Comparison between the leading-order and the next-to-leading-order contributions to the ^{113}Cd and ^{115}In decays

Theoretical analysis of the beta-decay observables is usually performed with the leading-order terms of the shape factor. This limits the number of nuclear matrix elements, and thus simplifies the application of the framework. A

particularly useful simplification is achieved with the unique decays where the decay rate is dependent on a single leading-order matrix element only. This results to the complete separation between the nuclear structure information and the kinematics. This separation is not attained with non-unique decays.

Finer details of the theory can be accessed when the framework is extended to the next-to-leading order[1]. The next-to-leading-order matrix elements are essentially derived from the leading-order elements by extra factors of $(r/R)^{2N}$ associated to the integrals of the single-particle matrix elements [16, 17]. However, extra coulomb factors are also needed to take into account the coulombic interaction (see details e.g. in Ref. [2]). These corrections increase the number of nuclear matrix elements from $2K + 4$ to $9K + 9$ for non-unigue K-forbidden decays. For unique decays of the same level of forbiddenness there is a total of $2K + 3$ matrix elements involved in the calculations. As a result, also the unique decays contain a mixture of vector and axial-vector components.

A comparison between the leading-order and the next-to-leading-order contributions to the beta-decay shape factor was performed in Refs. [1, 2] using the fourth-forbidden non-unique beta decays of ^{113}Cd and ^{115}In. Both decays have previously been studied e.g. in Ref. [38]. The experimental partial half-lives of these channels are measured to be $t^{\beta}_{1/2} = (8.04 \pm 0.05) \times 10^{15}$ yr and $t^{\beta}_{1/2} = (4.41 \pm 0.25) \times 10^{14}$ yr, respectively [36]. The Q-values of the two channels are (322 ± 1) keV and (497.489 ± 0.010) keV, respectively [36].

To inspect the dependence on the nuclear structure framework, the OBTDs of the beta-decay half-lives and spectra were calculated using two nuclear models in Ref. [1]. The selected models were the microscopic quasiparticle-phonon model (MQPM) and nuclear shell model (NSM). The effective interaction used in the NSM calculations was jj45pna [58, 59] which has recently been applied to $^{122-126}$Ag nuclei in Ref. [59]. Due to large dimensions, the NSM is prone to some truncation of the model space to ease the computational burden when applied to heavier nuclei. The details of the current NSM calculations are discussed in Ref. [1].

In Ref. [2] the original study was extended by performing the same OBTD calculations with the microscopic interacting boson-fermion model (IBFM-2,

[1]Other additional corrections that are beyond the usual application include e.g. the *radiative corrections*. These are a set of corrections that stem from the finer details of coulomb interaction. The division between *outer* and *inner* corrections is explained in Ref. [16]. The outer corrections that directly modify the shape factor are briefly discussed in Ref. [2].

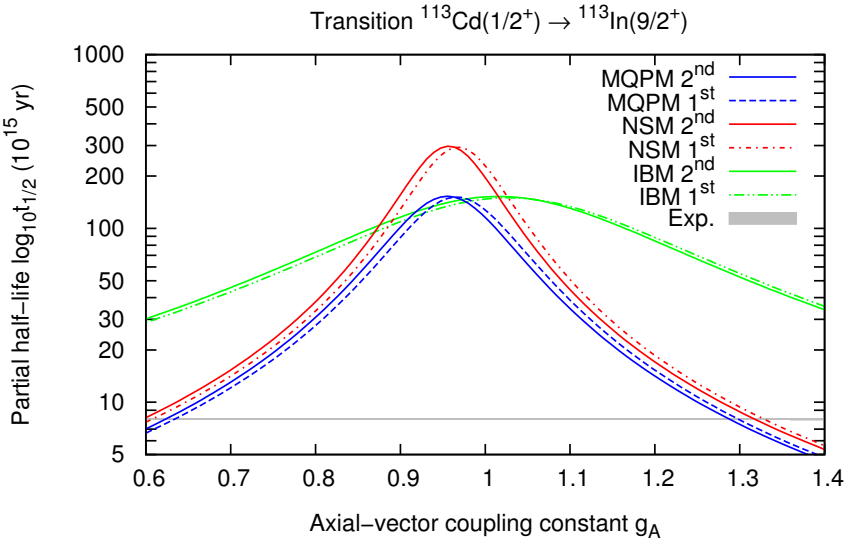

Figure 3.6: Partial half-life of the fourth-forbidden beta-decay branch of ^{113}Cd as a function of the value of the axial-vector coupling constant. The results calculated up to the next-to-leading-order (2^{nd}) are compared with the leading-order (1^{st}) contributions. The value of the vector coupling constant is $g_{\text{V}} = 1$, and the experimental half-life is presented as a gray horizontal line.

or simply IBM) [60, 61]. The parameters of the Cd core are taken from Ref. [62] in the current calculations.

A summary of the dependence of the partial half-life on the next-to-leading-order contributions is given in Figs. 3.6 - 3.9. All the three nuclear models show very similar behaviour when inspecting these effects as a function of the value of the axial-vector coupling constant. At highest these contributions can introduce an effect of around 20% to the partial half-life. In general the next-to-leading-order terms tend to increase the partial half-life at low values of g_A and reduce it when approaching the bare nucleon value. It is interesting to note that due to the very definite behaviour of the half-life curves in Figs. 3.6 and 3.7 the contribution of the next-to-leading-order terms can effectively be taken into account by a slight shift in the value of g_{A}.

Since the next-to-leading-order contributions affect also other beta-decay observables, the effects on the electron spectra can be inspected in similar ways. In general these contributions tend to be small, but at times there

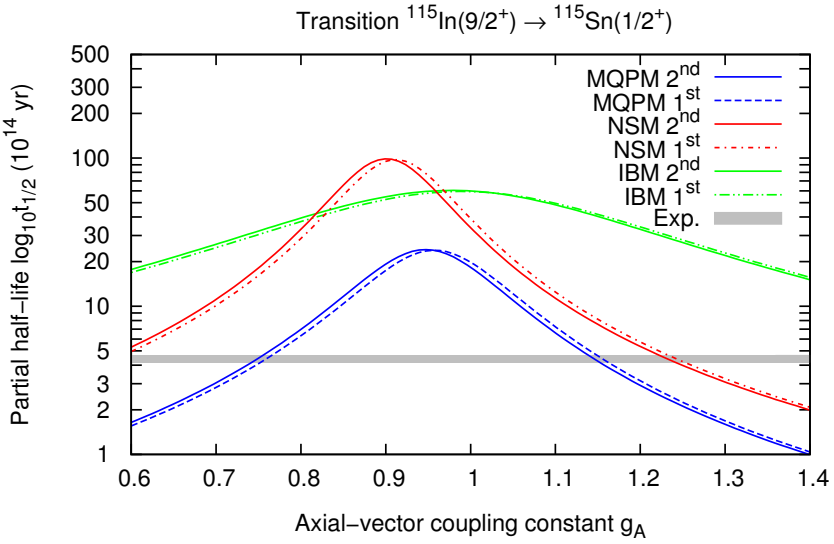

Figure 3.7: Partial half-life for the decay of ^{115}In (see the description of Fig. 3.6).

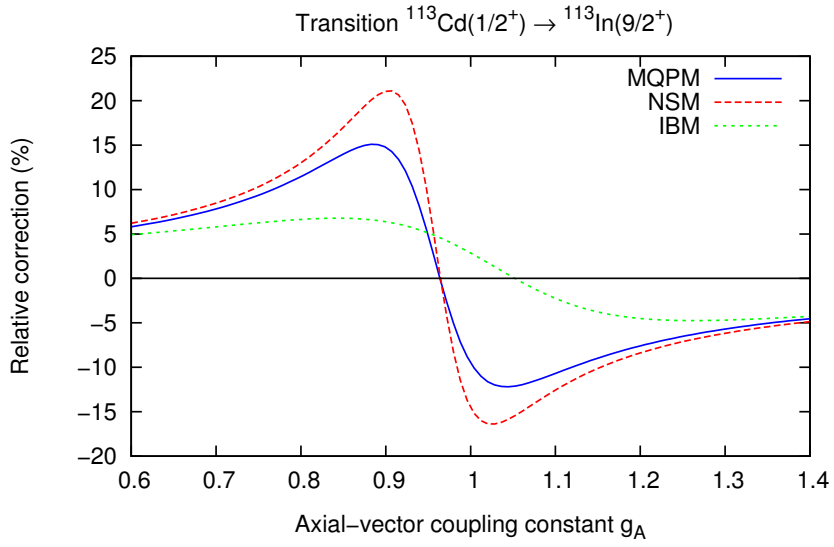

Figure 3.8: Effects of the next-to-leading-order contributions as functions of the value of the axial-vector coupling constant for the beta decay of ^{113}Cd. Relative corrections are extracted from the graphs in Fig. 3.6

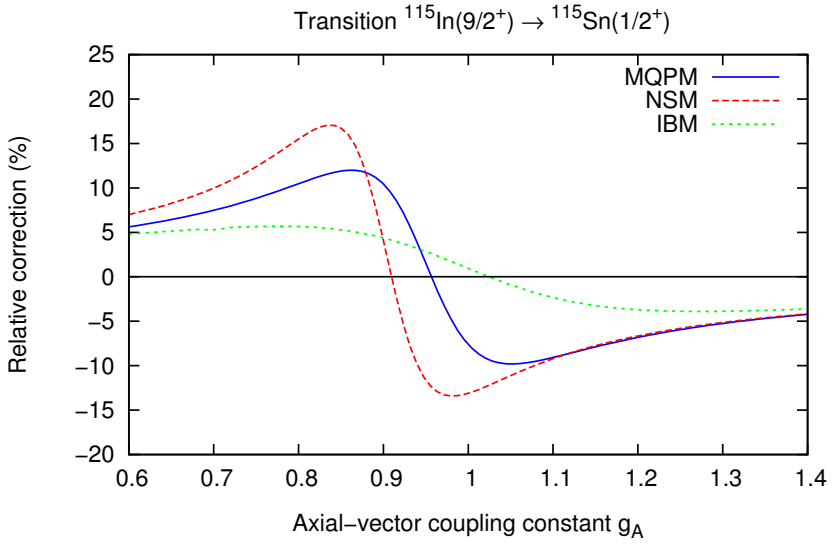

Figure 3.9: Effects of the next-to-leading-order contributions as functions of the value of the axial-vector coupling constant for the beta decay of ^{115}In. Relative corrections are extracted from the graphs in Fig. 3.7.

can be a fairly strong dependence on the values of the coupling constants. Fig. 3.10 represents the maximal effects that were recorded with the studies on the ^{113}Cd beta decay. The selected values of g_{A} are extracted from the peak-points of Fig. 3.8. Even when the effects are maximized, the next-to-leading-order contributions do not drastically alter the high-energy part of the spectrum. Most effects are seen to occur in lower energies, and at this energy range the contributions can amount up to 30%.

3.4 Spectrum-shape method

The usual method for the extraction of the effective values of the weak coupling constants involves studies on beta-decay half-lives. Since the beta-decay rate is affected by any adjustment of g_{V} and/or g_{A}, effective values of these constants can be probed by matching the theoretical half-life with the experiment. A particular interest is directed towards the effective values of the axial-vector coupling constant, and such studies have previously been performed in the context of the proton-neutron quasiparticle random-phase approximation (pnQRPA) in Refs. [7, 8, 23, 24, 63, 64, 65], NSM in Refs.

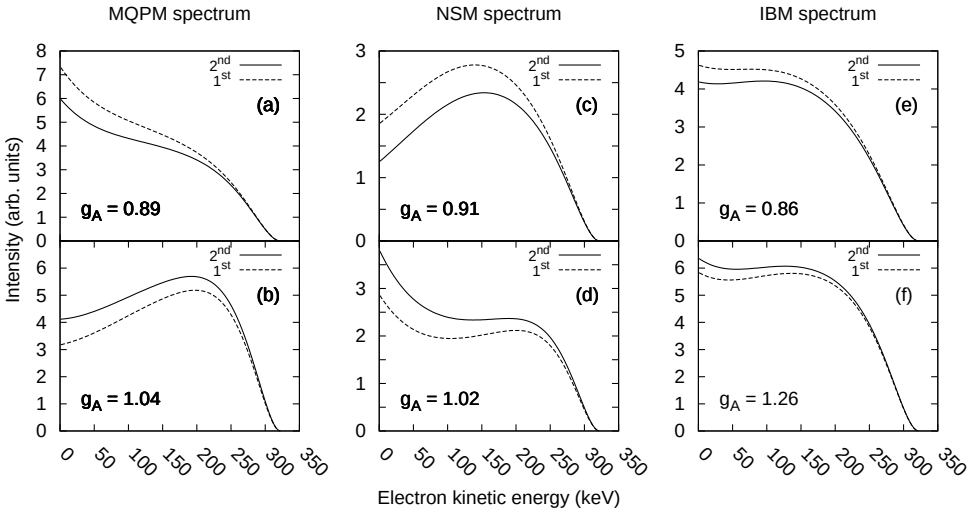

Figure 3.10: Extreme contributions of the next-to-leading-order terms of the beta-decay shape factor on the electron spectra of ^{113}Cd. The values of g_{A} (indicated in the figures) are extracted from Fig. 3.8.

[66, 67, 68] and IBM in Refs. [69, 70, 71]. These studies include various single- and double-beta-decay branches in medium heavy nuclei.

A complementary method for the extraction of the values of the weak coupling constants was first introduced in Ref. [1]. This method, called the spectrum-shape method (SSM), utilizes the information gained from the shape of the beta spectra through its non-trivial dependence on the values of g_{V} and g_{A}. Since the shape factor (2.28) of a non-unique decay (as well as that of a unique decay in next-to-leading order) can be decomposed into

$$C = g_{\mathrm{V}}^2 C_{\mathrm{V}} + g_{\mathrm{A}}^2 C_{\mathrm{A}} + g_{\mathrm{V}} g_{\mathrm{A}} C_{\mathrm{VA}}, \tag{3.1}$$

where C_{V}, C_{A} and C_{VA} are the vector, axial-vector and mixed components, respectively (see e.g. Refs. [2, 16]), the shape of the beta spectrum is also affected by the choice of these constants. Similar effect can also be observed in the decomposition of the integrated shape factor (2.30) which can be written as

$$\begin{aligned} \tilde{C} &= \int_{m_e c^2}^{W_0} C(W_e)\, p_e W_e (W_0 - W_e)^2\, F_0(Z, W_e) \mathrm{d}W_e \\ &= g_{\mathrm{V}}^2 \tilde{C}_{\mathrm{V}} + g_{\mathrm{A}}^2 \tilde{C}_{\mathrm{A}} + g_{\mathrm{V}} g_{\mathrm{A}} \tilde{C}_{\mathrm{VA}}. \end{aligned} \tag{3.2}$$

Thus effective values of the g_{V} and g_{A} pairs can be found by performing a comparison between theoretical and experimental beta spectra.

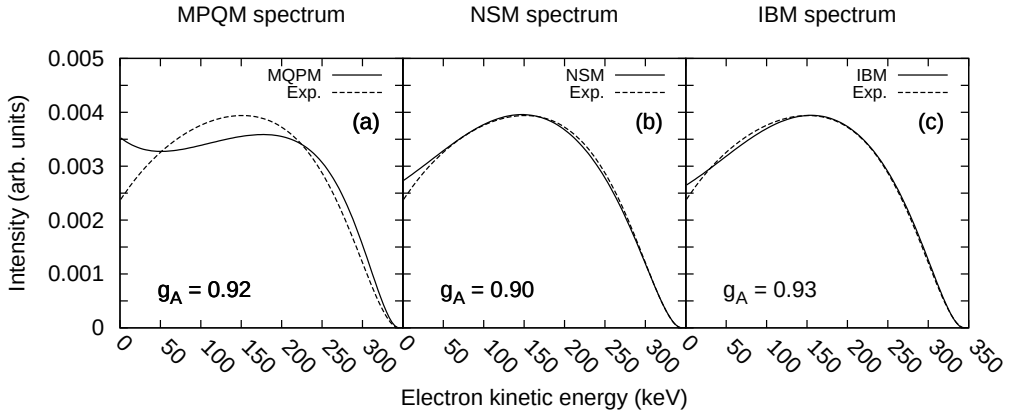

Figure 3.11: Comparison of the computed electron spectra of ^{113}Cd with the experimental data. The areas under the curves are normalized to unity. All calculations are performed using the next-to-leading-order contributions, and the value of the $g_{\rm V}$ was kept at unity. Note that the Q-value used in the SSM computations is (343.1 ± 0.6) keV to enable the comparison with the experimental data of Ref. [72].

In the pilot study of Ref. [1] SSM was applied to the non-unique fourth-forbidden beta decays of ^{113}Cd and ^{115}In. However, due to the lack of experimental data on the electron spectrum of ^{115}In, SSM was fully deployed only for ^{113}Cd. The electron spectrum of ^{113}Cd was earlier measured at the Gran Sasso National Laboratory using low-background $CdWO_4$ crystal scintillators [72]. The analysis performed in Ref. [1] with MQPM and NSM was further extended in Ref. [2], where the nuclear-structure calculations include also the use of IBM.

A comparison performed in Ref. [2] between the three nuclear models is summarized in Fig. 3.11. A highly interesting outcome of this analysis emerged: A consistent value of around $g_{\rm A} = 0.92$ can be used to reproduce the experimental electron spectra with all the three nuclear models. Although the MQPM-based fit shows some deviation from the experimental spectrum shape, the match attained with both the NSM and the IBM is excellent. Such a close agreement between all three nuclear models is a remarkable result considering the differences between their theoretical frameworks.

The significance of the results presented in Fig 3.11 is further emphasized by two other aspects. Firstly, the effective value $g_{\rm A} \approx 0.92$ is in a good agreement with the effective values of many other studies. Secondly, while the SSM value of $g_{\rm A}$ represents a fairly typical quenching of the axial-vector

Table 3.4: Effective values of g_A extracted from the beta decays of ^{113}Cd and ^{115}In (see Figs. 3.6, 3.7). The electron spectrum measured in Ref. [72] allows for the comparison between the partial-half-life-based and SSM-based effective values of g_A in the case of ^{113}Cd. Next-leading-order terms of the beta-decay shape factor were used to calculate all the results.

Nuclear model	Effective g_A				
	^{113}Cd			^{115}In	
	Half-life		SSM	Half-life	
MQPM	0.63	1.29	0.92	0.75	1.15
NSM	0.60	1.32	0.90	0.57	1.23
IBM	0.14	1.89	0.93	0.11	1.84

coupling constant, the preferred value of the vector coupling constant g_V turned out to be unity. In every decay branch examined in Refs. [7, 8, 23, 24, 63, 64, 65, 66, 67, 68, 69, 70, 71] the effective value of g_A was found to be quenched, i.e. it was less than the bare nucleon value $g_A = 1.27$. In most cases the effective value was, in fact, found to be less than unity. The second aspect is related to the validity of the CVC hypothesis. Although quenched values of the vector coupling constant are extracted e.g. in Refs. [73, 74] using shell-model studies on spin-dipole and other first-forbidden beta transitions (an extension to these studies was more recently achieved in Refs. [75, 76]), the SSM results seem to indicate the opposite. The preferred value of g_V was found to be its CVC value in the SSM studies using any of the nuclear models.

Despite the intriguing results of Fig. 3.11, a contradiction was found when the SSM results were compared with those of the partial half-life analysis (see Fig.3.6 in Sect. 3.3). This comparison is presented in Table 3.4. As a conclusion, it can be stated that the current SSM results do not agree well with the values extracted from the partial-half-life analysis. Although the discrepancies vary largely between the different nuclear models, the general trend is similar. In each case the SSM values lie in between the g_A pairs extracted from the partial half-lives.

It is important to understand that the beta decay of ^{113}Cd (and ^{115}In) is a non-unique transition. The parabolic dependence of the decay rate on g_A thus yields a total of two effective values of the coupling constant that correspond to the crossing points with the experimental partial half-life line (see Fig. 3.6). Contrary to this, the single-beta-decay studies in Refs. [7, 8, 23, 24, 63, 64, 65, 66, 67, 68] concentrate on unique or allowed transitions.

Both of these transitions yield only one effective value of $g_{\rm A}$. A further remark about the results of Table 3.4 can be made when comparing the values of $g_{\rm A}$ based on the partial half-life calculations with the other similar studies mentioned earlier. The lower values of $g_{\rm A}$ in Table 3.4 represent a fairly extreme quenching of the value of $g_{\rm A}$. The higher values, on the other hand, approach the bare nucleon value. The only exception is the IBM-based calculation that fails to produce any reasonable values at all.

The conflict between the SSM and half-life methods is not easily explained by any low-order corrections that are left out from the theoretical framework. Thus, *a priori*, there is no reason why the results of Table 3.4 should not converge when accurate nuclear matrix elements are used. The most obvious way to rectify the disagreement between the two methods would be to find a suitable set on nuclear matrix elements that brings the half-life curves of Fig. 3.6 down. This would not only make the half-life- and SSM-extracted values of $g_{\rm A}$ commensurate, but also lead to a unique effective value of $g_{\rm A}$, extracted from each half-life curve.

The fact that the two highly-forbidden non-unique decay transitions discussed in Ref. [2] are $g_{\rm A}$-sensitive inspires to speculate that this particular feature is shared by similar transitions in other nuclei. According to a more extensive study in Ref. [19] this expectation is not, however, entirely correct. In that article a total of 26 single-beta-decay transitions of varying forbiddenness were examined using the MQPM in connection with the SSM. Only three experimentally interesting candidates were found in that study.

The studies performed in Ref. [19] seem to support the observation that was already made in Refs. [1, 2]. Figs. 3.12 and 3.13, and Table 3.5 show that the strong dependence on $g_{\rm A}$ (or $g_{\rm V}$) is a result of the competition between the vector and axial-vector components of the shape factor in Eq. (3.1). When these components are of the same order of magnitude any small variation in the values of the weak coupling constants is able to change the balance between these components. In Ref. [19] this feature (see the results of Table 2 in Ref. [19]) was found from the decay transition $^{99}{\rm Tc}(9/2^+) \rightarrow {}^{99}{\rm Ru}(5/2^+)$ which is of a non-unique second-forbidden type. Other decays with similar characteristics include the non-unique forth-forbidden transitions $^{115}{\rm Cd}(1/2^+) \rightarrow {}^{115}{\rm In}(9/2^+)$, $^{117}{\rm Cd}(1/2^+) \rightarrow {}^{117}{\rm In}(9/2^+)$ and $^{119}{\rm In}(9/2^+) \rightarrow {}^{119}{\rm Sn}(1/2^+)$. All these decay branches would serve as highly interesting candidates for further SSM studies if the electron spectra could be measured experimentally.

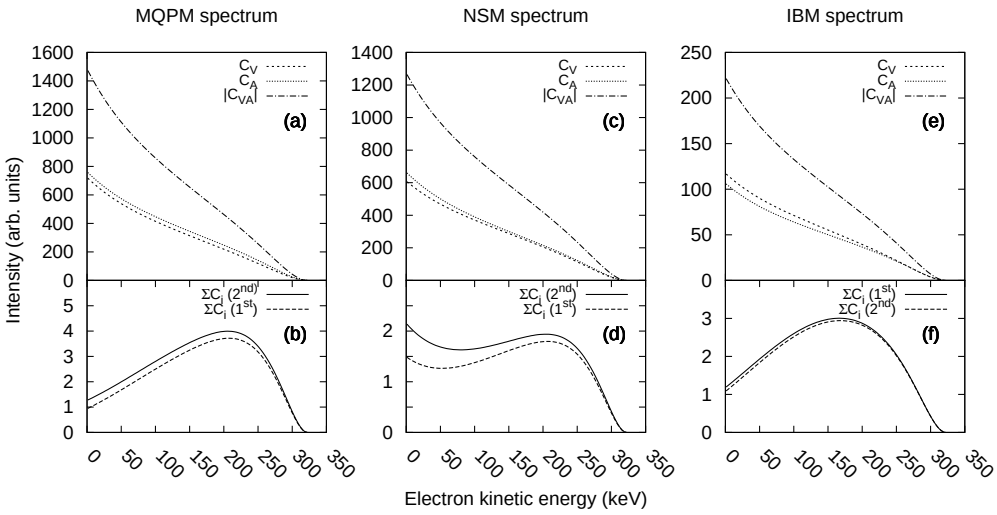

Figure 3.12: Decomposed electron spectra of the ^{113}Cd beta decay $^{113}\mathrm{Cd}(1/2^+) \rightarrow {}^{113}\mathrm{In}(9/2^+)$. The vector ($C_\mathrm{V}$), axial-vector ($C_\mathrm{A}$) and mixed term ($C_\mathrm{VA}$) of the shape factor are presented in the upper panels including the next-to-leading-order corrections. The lower panels represent the sum, i.e. the total shape factor. Comparison to the leading-order contributions (abbreviated by 1$^{\mathrm{st}}$) is performed in each of the lower panels. Notice that the sign of the mixed term C_VA is negative.

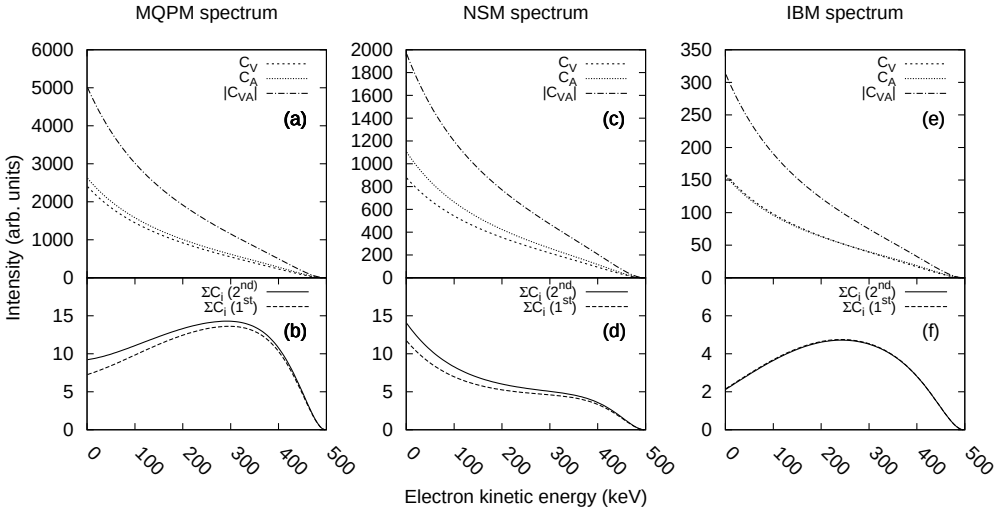

Figure 3.13: Decomposed electron spectra of the ^{115}In beta decay $^{115}\mathrm{In}(9/2^+) \rightarrow {}^{115}\mathrm{Sn}(1/2^+)$ (see the description of Fig. 3.12).

Table 3.5: Comparison between the vector ($\tilde{C}_V$), axial-vector ($\tilde{C}_A$) and mixed ($\tilde{C}_{VA}$) terms of the integrated shape factor (3.2). The sum of these three terms (see the last row) is the total integrated shape factor for $g_{\rm V} = g_{\rm A} = 1$. All the calculations are performed using the next-to-leading-order corrections, and all the values are given in units of 10^{-20}.

	^{113}Cd$(1/2^+) \rightarrow {}^{113}In(9/2^+)$			^{115}In$(9/2^+) \rightarrow {}^{115}Sn(1/2^+)$		
	MQPM	NSM	IBM	MQPM	NSM	IBM
$\tilde{C}_V$	19.247	16.783	3.228	829.927	314.577	55.314
$\tilde{C}_A$	20.940	18.254	3.007	916.121	385.083	54.438
$\tilde{C}_{VA}$	-40.019	-34.939	-6.106	-1735.4	-693.914	-106.501
$\sum \tilde{C}_i$	0.169	0.099	0.128	10.642	5.745	3.251

4 Summary

In this thesis a set of well-established and extensively tested theoretical frameworks were used to gain information on specific cases of rare beta decays. These studies included the investigation of the possible ultra-low-Q-value beta-decay transition of ^{115}Cd, and the highly-forbidden beta decays of ^{48}Ca, ^{50}V, ^{113}Cd and ^{115}In. In addition to this direct application of the theory, the aim of the thesis work was also to extend the established toolset. This included studies of to the next-to-leading-order contributions to the beta-decay shape factor, and the introduction of the *spectrum-shape method*.

Beta decay serves as a useful testbench for any nuclear models since these decays are abundant all over the nuclear landscape. When examining the performance of the three nuclear models, i.e. the microscopic quasiparticle-phonon model (MQPM), the nuclear shell model (NSM) and the interacting boson-fermion model (IBFM), used in the current work to describe the initial and final nuclear states of the decay transitions, a fairly satisfactory agreement between the theory and experiment was found in general. This concerns both the spectroscopic properties of the nuclei as well as the resulting half-life estimates.

The possible ultra-low Q-value of the transition $^{115}\mathrm{Cd}(1/2^+_{\mathrm{g.s.}}) \rightarrow {}^{115}\mathrm{In}(9/2^+_3)$ is a highly desired feature when considering direct studies of the neutrino rest-mass. However, the usability of this particular transition is hampered by its extensively long partial half-life. Thus any practical use of the transition for this purpose seems unlikely. Despite the very limited usage for the neutrino studies, this and the other similar ultra-low-Q-value decays can still serve as possible candidates for the studies of atomic interference effects in nuclear decay.

The current theoretical studies of the highly-forbidden single beta-minus-decay channels of ^{48}Ca and ^{50}V offer reliable information on the experimental detectability of these decays. In the case of ^{48}Ca the computed partial half-life of the single beta-decay channel was found to be 53% shorter than that of to the previous study. This indicates a slightly stronger competition between the single- and double-beta-decay channels, but confirms that the double-beta channel is still relatively weakly challenged by the single beta decay. In the case of ^{50}V the current computed estimate for the partial half-life of the beta-minus decay seems to suggest that an improved experimental set-up could be fairly easily devised for the verification of this transition. At

the same time the current prediction is in a strong conflict with the single claimed observation of this decay branch in the past.

The initial results obtained for the highly-forbidden beta decay of ^{113}Cd seem to suggest that the spectrum-shape method (SSM) offers highly interesting potential for the studies of the effective values of the weak coupling constants. This method complements well the usual partial-half-life considerations due to the fact that the dependence between the shape of the beta spectrum and the values of the weak coupling constants is directly linked through the competition between the vector and axial-vector parts of the shape factor. When the vector and axial-vector components are of the same order of magnitude, any small adjustments of the values of the weak coupling constants can result to a noticeable effect in the spectrum shape.

According to the studies on the ^{113}Cd and ^{115}In beta decays, SSM, as well as any other calculations of the beta-decay observables, can benefit from the extension of the beta-decay formalism to the next-to-leading-order terms of the shape factor. The effects of these contributions are generally moderate, but they depend on the values of the weak coupling constants. The strongest effects are seen in the low-energy part of the beta spectrum.

Bibliography

[1] M. Haaranen, P. C. Srivastava, J. Suhonen, Phys. Rev. C **93**, 034308 (2016)

[2] M. Haaranen, J. Kotila, J. Suhonen, Phys. Rev. C **95**, 024327 (2017)

[3] M. Haaranen, M. Horoi, J. Suhonen, Phys. Rev. C **89**, 034315 (2014)

[4] M. Haaranen, P. C. Srivastava, J. Suhonen, K. Zuber, Phys. Rev. C **90**, 044314 (2014)

[5] J. Suhonen, O. Civitarese, Phys. Rep. **300**, 123 (1998)

[6] J. Maalampi, J. Suhonen, Adv. High Energy Phys. **2013**, 505874 (2013)

[7] H. Ejiri, N. Soukouti, J. Suhonen, Phys. Lett. B **729**, 27 (2014)

[8] H. Ejiri, J. Suhonen, J. Phys. G: Nucl. Part. Phys. **42**, 055201 (2015)

[9] F. T. Avignone III, S. R. Elliott, J. Engel, Rev. Mod. Phys. **80**, 481 (2008)

[10] F. Schwamm, AIP Conf. Proc. **605**, 461 (2002)

[11] G. Drexlin, V. Hannen, S. Mertens, C. Weinheimer, Adv. High Energy Phys. **2013**, 293986 (2013)

[12] M. Haaranen, J. Suhonen, Eur. Phys. J. A **49**, 93 (2013)

[13] M. T. Mustonen, M. Aunola, J. Suhonen, Phys. Rev. C **73**, 054301 (2006)

[14] M. Aunola, J. Suhonen, T. Siiskonen, Europhys. Lett. **46**, 577 (1999)

[15] H. Heiskanen, M. T. Mustonen, J. Suhonen, J. Phys. G: Nucl. Part. Phys. **34**, 837 (2007)

[16] H. Behrens, W. Bühring, *Electron Radial Wave Functions and Nuclear Beta-decay* (Clarendon Press, Oxford, 1982)

[17] H. F. Schopper, *Weak Interaction and Nuclear Beta Decay* (North-Holland, Amsterdam, 1966)

[18] J. Suhonen, *From Nucleons to Nucleus: Concepts of Microscopic Nuclear Theory* (Springer, Berlin, 2007)

[19] J. Kostensalo, M. Haaranen, J. Suhonen, Phys. Rev. C **95**, 044313 (2017)

[20] F. Halzen, A. D. Martin, *Quarks and Leptons: An Introductory Course in Modern Particle Physics* (John Wiley & Sons, United Kingdom, 1984)

[21] E. D. Commins, *Weak interactions* (McGraw-Hill, New York, 2007)

[22] A. Bohr, B. R. Mottelson, Phys. Lett. B **100**, 10 (1981)

[23] J. Suhonen, O. Civitarese, Phys. Lett. B **725**, 153 (2013)

[24] J. Suhonen, O. Civitarese, Nucl. Phys. A **924**, 1 (2014)

[25] B. Stech, L. Schülke, Z. Physik **179**, 314 (1964)

[26] M. Wang, G. Audi, F. G. Kondev, W. J. Huang, S. Naimi, X. Xu, Chin. Phys. C **41**, 030003 (2017)

[27] B. J. Mount, M. Redshav, E. G. Myers, Phys. Rev. Lett. **103**, 122502 (2009)

[28] W. Urban, U. Köster, M. Jentschel, P. Mutti, B. Märkisch, T. Rząca-Urban. Ch. Bernards, Ch. Fransen, J. Jolie, T. Thomas, G. S. Simpson, Phys. Rev. C **94**, 011302 (2016)

[29] E. Andreotti, M. Hult, R. González de Orduña, G. Marissens, J. S. E. Wieslander, M. Misiaszek, Phys. Rev. C **84**, 044605 (2011)

[30] J. S. E. Wieslander, J. Suhonen, T. Eronen, M. Hult, V. Elomaa, A. Jokinen, G. Marissens, M. Misiaszek, M. T. Mustonen, S. Rahaman, C. Weber, J. Äystö, Phys. Rev. Lett. **103**, 122501 (2009)

[31] M. T. Mustonen, J. Suhonen, Phys. Lett. B **703**, 370 (2011)

[32] J. Suhonen, O. Civitarese, J. Phys. G: Nucl. Part. Phys. **39**, 085105 (2012)

[33] J. Suhonen, O. Civitarese, J. Phys. G: Nucl. Part. Phys. **39**, 124005 (2012)

[34] M. T. Mustonen, J. Suhonen, J. Phys. G: Nucl. Part. Phys. **37**, 064008 (2010)

[35] J. Suhonen, M. T. Mustonen, Prog. Part. Nucl. Phys. **64**, 235 (2010)

[36] ENSDF at NNDC site, http://www.nndc.bnl.gov

[37] J. Toivanen, J. Suhonen, Phys. Rev. C **57**, 1237 (1998)

[38] M. T. Mustonen, J. Suhonen, Phys. Lett. B **657**, 38 (2007)

[39] A. Poves, Phys. Lett. B **361**, 1 (1995)

[40] J. Suhonen, J. Phys. G: Nucl. Part. Phys. **19**, 139 (1993)

[41] A. Balysh, A. De Silva, V. I. Lebedev, K. Lou, M. K. Moe, M. A. Nelson, A. Piepke, A. Pronskiy, M. A. Vient, P. Vogel, Phys. Rev. Lett. **77**, 5186 (1996)

[42] A. S. Barabash, Nucl. Phys. A **935**, 52 (2015)

[43] A. Bakalyarov, A. Balysh, A. Barabash, Ch. Briançon, V. Brudanin, V. Egorov, F. Hubert, Ph. Hubert, A. Kovalik, V. I. Lebedev, N. I. Rukhadze, I. Štekl, V. Umatov, Ts. Vylov, Nucl. Phys. A **700**, 17 (2002)

[44] A. Bakalyarov, A. Balysh, A. Barabash, P. Beneš, Ch. Briançon, V. Brudanin, P. Čermák, V. Egorov, F. Hubert, Ph. Hubert, N. A. Korolev, V. N. Kosjakov, A. Kovalik, N. A. Lebedev, V. I. Lebedev, A. F. Novgorodov, N. I. Rukhadze, I. Štekl, V. V. Timkin, I. E. Veleshko, Ts. Vylov, V. I. Umatov, JETP Lett. **76**, 545 (2002)

[45] A. S. Barabash, R. Gurriaran, F. Hubert, Ph. Hubert, J. L. Reyss, J. Suhonen, V. Umatov, J. Phys. G: Nucl. Part. Phys. **22**, 487 (1996)

[46] R. Arnold, C. Augier, J. Baker, A. Barabash, D. Blum, V. Brudanin, A. J. Caffrey, J. E. Campagne, E. Caurier, D. Dassie, V. Egorov, T. Filipova, R. Gurriaran, J. L. Guyonnet, F. Hubert, Ph. Hubert, S. Jullian, I. Kisel, O. Kochetov, V. N. Kornoukhov, V. Kovalenko, D. Lalanne, F. Laplanche, F. Leccia, I. Linck, C. Longuemare, Ch. Marquet, F. Mauger, H.W. Nicholson, I. Pilugin, F. Piquemal, J-L. Reyss, X. Sarazin, F. Scheibling, J. Suhonen, C. S. Sutton, G. Szklarz, V. Timkin, R. Torres, V.I. Tretyak, V. Umatov, I. Vanyushin, A. Vareille. Yu. Vasilyev. Ts. Vylov, Nucl. Phys. A **658**, 299 (1999)

[47] E. K. Warburton, Phys. Rev. C **31**, 1896 (1985)

[48] E. K. Warburton, Phys. Rev. C **45**, 463 (1992)

[49] M. Honma, T. Otsuka, B. A. Brown, T. Mizusaki, Phys. Rev. C **69**, 034335 (2004)

[50] M. Honma, T. Otsuka, B. A. Brown, T. Mizusaki, Eur. Phys. J. A **25**, 499 (2005)

[51] P. F. Mantica, R. Broda, H. L. Crawford, A. Damaske, B. Fornal, A. A. Hecht, C. Hoffman, M. Horoi, N. Hoteling, R. V. F. Janssens, J. Pereira, J. S. Pinter, J. B. Stoker, S. L. Tabor, T. Sumikama, W. B. Walters, X. Wang, and S. Zhu, Phys. Rev. C **77**, 014313 (2008)

[52] M. Horoi, S. Stoica, B. A. Brown, Phys. Rev. C **75**, 034303 (2007)

[53] M. Horoi, S. Stoica, Phys. Rev. C **81**, 024321 (2010)

[54] M. Horoi, Phys. Rev. C **87**, 014320 (2013)

[55] L. S. Brown, Phys. Rev. **135**, B314 (1964)

[56] H. Dombrowski, S. Neumaier, K. Zuber, Phys. Rev. C **83**, 054322 (2011)

[57] J. J. Simpson, P. Moorhouse, P. Jagam, Phys. Rev. C **39**, 2367 (1989)

[58] R. Machleidt, Phys. Rev. C **63**, 024001 (2001)

[59] S. Lalkovski, A. M. Bruce, A. Jungclaus, M. Gorska, M. Pfützner, L. Caceres, F. Naqvi, S. Pietri, Zs. Podolak, G. S. Simpson, K. Andgren, P. Bednarczyk, T. Beck, J. Benlliure, G. Benzoni, E. Casarejos, B. Cederwall, F. C. L. Crespi, J. J. Cuenca-García, I. J. Cullen, A. M. Denis Bacelar, P. Detistov, P. Doornenbal, G. F. Farrelly, A. B.Garnsworthy, H. Geissel, W. Gelletly, J. Gerl, J. Grebosz, B. Hadinia, M. Hellström, C. Hinke, R. Hoischen, G. Ilie, G. Jaworski, J. Jolie, A. Khaplanov, S. Kisyov, M. Kmiecik, I. Kojouharov, R. Kumar, N. Kurz, A. Maj, S. Mandal, V. Modamio, F. Montes, S. Myalski, M. Palacz, W. Prokopowicz, P. Reiter, P. H. Regan, D. Rudolph, H. Schaffner, D. Sohler, S. J. Steer, S. Tashenov, J. Walker, P. M. Walker, H. Weick, E. Werner-Malento, O. Wieland, H. J. Wollersheim, M. Zhekova, Phys. Rev. C **87**, 034308 (2013)

[60] F. Iachello, A. Arima, *The interacting boson model* (Cambridge University Press, Great Britain, 1987)

[61] F. Iachello, P. Van Isacker, *The interacting boson-fermion model* (Cambridge University Press, United States of America, 1991)

[62] A. Giannatiempo, A. Nannini, A. Perego, P. Sona, G. Maino, Phys. Rev. C **44**, 1508 (1991)

[63] A. Faessler, G. L. Fogli, E. Lisi, V. Rodin, A. M. Rotunno, F. Šimkovic, J. Phys. G: Nucl. Part. Phys. **35**, 075104 (2008)

[64] D. S. Delion, J. Suhonen, Europhys. Lett. **107**, 52001 (2014)

[65] P. Pirinen, J. Suhonen, Phys. Rev. C **91**, 054309 (2015)

[66] B. H. Wildenthal, M. S. Curtin, B. A. Brown, Phys. Rev. C **28**, 1343 (1983)

[67] G. Martínez-Pinedo, A. Poves, E. Caurier, A. P. Zuker, Phys. Rev. C **53**, R2502 (1996)

[68] E. Caurier, F. Nowacki, A. Poves, Phys. Lett. B **711**, 62 (2012)

[69] J. Barea, J. Kotila, F. Iachello, Phys. Rev. C **87**, 014315 (2013)

[70] J. Barea, J. Kotila, F. Iachello, Phys. Rev. C **91**, 034304 (2015)

[71] N. Yoshida, F. Iachello, Prog. Theor. Exp. Phys. **2013**, 043D01 (2013)

[72] P. Belli, R. Bernabei, N. Bukilic, F. Cappella, R. Cerulli, C. J. Dai, F. A. Danevich, J. R. de Laeter, A. Incicchitti, V. V. Kobychev, S. S. Nagorny, S. Nisi, F. Nozzoli, D. V. Poda, D. Prosperi, V. I. Tretyak, S. S. Yurchenko, Phys. Rev. C **76**, 064603 (2007)

[73] E. K. Warburton, Phys. Rev. C **42**, 2479 (1990)

[74] E. K. Warburton, Phys. Rev. C **44**, 233 (1991)

[75] T. Suzuki, T. Yoshida, T. Kajino, T. Otsuka, Phys. Rev. C **85**, 015802 (2012)

[76] Q. Zhi, E. Caurier, J. J. Cuenca-García, K. Langanke, G. Matrínez-Pinedo, K. Sieja, Phys. Rev. C **87**, 025803 (2013)